IB 2022-105

An Empirical Wall Law for the Mean Velocity in Adverse Pressure Gradients

Tobias Knopp

DLR Deutsches Zentrum für Luft- und Raumfahrt

Berichts.-Nr.: **DLR-IB-AS-GO-2022-105**

Verfasser: Tobias Knopp

Titel: An Empirical Wall Law for the Mean Velocity in Adverse Pressure Gradients

Datum:

Auftraggeber:

Auftrags-Nr.:

Vorgesehen für:

Der Bericht umfaßt:

57 Seiten einschl.
4 Tabellen
24 Bilder
75 Literaturstellen

D L R

Institut für Aerodynamik und Strömungstechnik
Bunsenstraße 10
37073 Göttingen
Deutschland

Abteilung AS-CAS

DLR

Titel: An Empirical Wall Law for the Mean Velocity in Adverse Pressure Gradients

An empirical wall law for the mean velocity in an adverse pressure gradient is presented, with the ultimate goal of aiming at the improvement of RANS turbulence models and wall functions. For this purpose a large database of turbulent boundary-layer flows in adverse pressure gradients from wind tunnel experiments is considered, and the mean velocity in the inner layer is analysed. The log law in the mean velocity is found to be a robust feature. The extent of the log-law region is reduced in ratio to the boundary layer thickness with increasing strength of the pressure gradient. An extended wall law emerges above the log law, extending up to the outer edge of the inner layer. An empirical correlation to describe the reduction of the log-law region is proposed, depending on the pressure-gradient parameter and on the Reynolds number in inner viscous scaling, whose functional form is motivated by similarity and scaling arguments. Finally, there is a discussion of the conjecture of the existence of a wall law for the mean velocity, which is governed mainly by local parameters and whose leading order effects are the pressure gradient and the Reynolds number, but whose details can be perturbed by higher-order local and history effects.

DEUTSCHES ZENTRUM FÜR LUFT- UND RAUMFAHRT E.V.

Institut für Aerodynamik und Strömungstechnik

Institutsleiter:

(Prof. Dr. Andreas Dillmann)

Verfasser:

T. Knopp

(Dr. Tobias Knopp)

Abteilungsleiter:

(Dr. Cornelia Grabe)

Datum: 24.10.22	**Abteilung:**	**Bericht:**
Bearbeitet:	AS-CAS	IB-AS-GO-2022-105

Contents

Chapter 1

Introduction

Significant uncertainties are still associated with predicting of turbulent boundary-layer flows over smooth surfaces subjected to an adverse pressure gradient (APG) and flow separation using statistical turbulence models based on the Reynolds-averaged Navier-Stokes (RANS) equations. These flows have a high relevance in many technical applications, e.g., for the flow around aircraft wings, turbomachinery blades, and wind turbine blades. Among these flows, the flows around aircraft are special due to their high Reynolds numbers and their large ratio of surface area to boundary-layer thickness. This makes turbulence-resolving methods extremely expensive even for a single flow simulation Spalart [2015], whereas a great many simulations are needed for CFD-based configurative design and optimization of new aircraft concepts. Moreover, improvements of RANS models in the inner part of the boundary layer are important for large-eddy simulation (LES) with wall functions (see Tessicini et al. [2007]) and hybrid RANS/LES methods based on the detached-eddy-simulation approach (see Shur et al. [2008]). The lack of knowledge about an empirical wall law for the mean velocity in an adverse pressure gradient is a primary hurdle for the improvement of RANS turbulence models.

For turbulent boundary-layer flows at zero pressure gradient, there is a wide consensus that the mean velocity U in the inner part of the boundary layer at sufficiently large Reynolds numbers can be described by the log law (see Marusic et al. [2013])

$$u^+ = \frac{1}{\kappa}\log(y^+) + B\,. \tag{1.1}$$

Here y is the wall-distance, and inner viscous scaling $u^+ = U/u_\tau$, $y^+ = yu_\tau/\nu$ is used with the wall shear stress τ_w, the density ρ, the friction velocity $u_\tau = \sqrt{\tau_w/\rho}$, and the kinematic viscosity ν. The outer edge of the region occupied by the log law is near $y = 0.15\delta$, with δ being determined from a fit of the composite law-of-the-wall/law-of-the-wake Marusic et al. [2013]. The region $y < 0.15\delta$ will be referred to as the inner layer.

The resilience of the log law for the mean velocity in an APG is widely reported in Coles and Hirst [1969], Galbraith et al. [1977], Perry et al. [1966], Alving and Fernholz [1995], and Johnstone et al. [2010]. The region occupied by the log law in ratio to δ is found to be reduced, compared to the zero-pressure-gradient case, as the effect of the APG, e.g., the pressure-gradient parameter in inner

viscous scaling

$$\Delta p_s^+ = \nu/(\rho u_\tau^3)\mathrm{d}P/\mathrm{d}s \tag{1.2}$$

becomes stronger (see Alving and Fernholz [1995], Knopp [2016]). Here P is the pressure and s is the wall-tangential direction of the mean velocity as $y \to 0$ (see section 2.1). Some researchers report that a so-called half-power law or square-root law (abbreviated: sqrt-law) emerges above the log law (see Perry et al. [1966], Kader and Yaglom [1978], and Telbany and Reynolds [1980], and Nakabayashi et al. [2004]). To be more precise, these authors used the half-power law for zero-skin-friction flow by Stratford [1959] (given in equation (2.13) in section 2.3). Note that the half-power law is related to the y-scaling of the mixing length (see Stratford [1959]). This distance-from-the-wall scaling was recently found for the turbulent structures of the APG flow by Romero et al. [2022]. Alternatively, an extended wall law was applied in the entire inner layer above the buffer layer (see Szablewski [1960], Townsend [1961], and Afzal [2008]), which is asymptotic to the log law at low values of Δp_s^+ and asymptotic to the half-power law at large values of Δp_s^+. (The extended wall law is given in equation (2.12) in section 2.3). The extended wall law was used in Knopp et al. [2021] to describe the mean velocity above the log law in an APG. In Knopp et al. [2021] and in the present work, the designation "half-power law" is used loosely for the extended wall law (2.12)).

Regarding the breakdown of the log law in an APG, the work by Alving and Fernholz [1995] supports the idea of a breakdown if Δp_s^+ exceeds some threshold, e.g., $\Delta p_s^+ > 0.05$, rather than the onset of instantaneous reverse flow. The breakdown of a region where u^+ grows linearly with $\log(y^+)$ needs to be distinguished from a change of κ and B. Regarding the latter, some theoretical results and experimental observations indicate that the values for κ and B could change for strong values of Δp_s^+ (see Nickels [2004], Dixit and Ramesh [2008], and Knopp et al. [2021]). This question is not studied in the present work, mainly due to the significant effect of the accuracy to determine u_τ on the values inferred for κ (see Knopp et al. [2021]).

The great question is the existence of a wall-law region in which the mean-velocity profile depends only on local flow quantities. Such a region was proposed, among others, by Perry et al. [1966], who divided the boundary layer into a wall region and a historical region. In the wall region, only the local flow quantities/variables $(1/\rho)\mathrm{d}P/\mathrm{d}s$, τ_w/ρ, ν, and y govern the mean-velocity profile, and higher derivatives of $(1/\rho)\mathrm{d}P/\mathrm{d}s$ and τ_w/ρ could be involved above a certain wall-distance. In the historical region, the mean-velocity profile is influenced by upstream events. The existence of a local wall law can be motivated by and is related to the concept of moving equilibrium. Following Kader and Yaglom [1978], a boundary-layer flow is in moving equilibrium if the free-stream velocity U_∞ and the kinematic pressure gradient $(1/\rho)\mathrm{d}P/\mathrm{d}s$ are varying only slowly with the streamwise coordinate s so that the boundary layer adjusts to these variations and its structure at any value of s depends essentially on the relevant local parameters (at the same s) only, not on the upstream history of the flow.

Similar results were found for Couette-Poiseuille (CP) flow by Telbany and Reynolds [1980], reporting that the logarithmic layer is eroded, and ultimately vanishes, as the stress gradient increases in importance. Here the wall-normal stress gradient is given by the streamwise pressure gradient. Similar results

were found by Nakabayashi et al. [2004]. Moreover, a correlation is reported for the y^+-location of transition between the logarithmic layer and the so-called gradient layer (being the half-power law region), i. e., $y^+ = 90\lambda^{-1/2}$ using the parameter $\lambda = \Delta p_s^+ Re_{\tau,h}$, with $Re_{\tau,h}$ based on u_τ and on the channel half-width h. The systematic reduction of the log-law region and the appearance of a half-power law for CP flow can therefore be seen as a consequence of the pressure gradient and not a history effect, as CP flow is a self-similar flow in dynamic equilibrium in the sense of Gungor et al. [2016]. The findings for CP flow are seen to support the conjecture of a local wall law.
The present paper describes the first part of a strategy to modify RANS models for APGs. The strategy consists of three steps:

1. Set-up of a database of turbulent boundary-layer flows in an APG;
2. Development of an (empirical) wall law in an APG;
3. Modification of RANS models to account for the wall law in an APG.

The first two steps are described in the present paper. The third step will be described in a separate paper.
The present approach to find a wall law in an APG uses a combination of data analysis and theoretical arguments. A large database from wind tunnel experiments was analysed. The initial preliminary results were presented in Knopp [2016]. The core of the database is the famous test case collection Coles and Hirst [1969] published at the seminal 1968 Stanford conference on the computation of turbulent boundary layers. In this database, only a few mean-velocity profiles are for large values of $\Delta p_s^+ > 0.01$ at high Re.
As a remedy, a series of joint DLR/UniBw turbulent boundary-layer experiments have been performed since 2011. The geometry model that produces a strong APG consists of a diffuser type wall segment with convex streamwise curvature which smoothly joins a flat plate at opening angles of 13.0° and 14.4°, and 18.6° with respect to the wind tunnel wall in the three experiments. The flat plate is the APG focus region. The first experiment was at Δp_s^+ up to 0.05 and Re_θ up to 18000 (see Knopp et al. [2015]). A small log-law region was indicated from the diagnostic function for the log law, and a half-power law was observed above the log law, albeit only over a small region in terms of y^+. In the second experiment, large values of Re_θ up to 60000 were reached. A half-power law region was found from the diagnostic function for the half-power law (see Knopp et al. [2021]). The values for Δp_s^+ were reduced to below 0.03 so that the flow was remote from separation. In the third experiment, the APG was increased, leading to separation. Preliminary results are shown in Knopp et al. [2022].
Analysis of the database prompts the following hypotheses about an empirical wall law for the mean velocity in an adverse pressure gradient:

- The log law in the mean-velocity profile is a robust feature in an APG;
- The log-law region is thinner than its zero-pressure-gradient counterpart at the same Re_τ and does not extend up to $y = 0.15\delta$;
- The extent of the log-law region in ratio to δ is decreasing with increasing Δp_s^+;

- An extended wall law (designated loosely as "half-power law") emerges above the log law in a large part of the region the log law occupies at zero pressure gradient.

Note that an additional hypothesis states that the von Kármán constant κ changes with Δp_s^+ and that this can be described by the model by Nickels [2004]; however, this is not considered in the present work. In the present paper, the focus is directed at the mean velocity in the inner part of turbulent boundary layers. Recent work focusing mainly on the outer part of the boundary layer in an adverse pressure gradient can be found in Romero et al. [2022], Maciel et al. [2018], Bobke et al. [2017], Vila et al. [2017], and Vila et al. [2020]. This work is restricted to turbulent boundary-layer flows. Internal flows with streamwise pressure gradients like Couette-Poiseuille flows (Telbany and Reynolds [1980]) or flows in divergent channels (Szablewski [1954]) are not considered. The analysis is restricted to the case of plane-wall, two-dimensional flow. Effects of streamwise curvature are ignored. The effects of three-dimensional boundary-layer flows with sweep (Coleman et al. [2019]) and cases with a three-dimensionality of the flow due to a spanwise expansion of the geometry or spanwise surface curvature are excluded. Streamwise curvature leads to a departure from the log law which is increasing with increasing y^+. The profile for u^+ turns below the log law in the case of a concave wall and above in the case of a convex wall (see Kim and Rhode [2000]). In three-dimensional turbulent boundary layer flows, a streamwise and a spanwise component of the mean velocity arise (defined in a local coordinate system with the x-axis aligned with the freestream or with the wall shear stress vector), and a spanwise pressure gradient results in flow skewing (see Devenport and Lowe [2022]). A wall law for the mean-velocity component aligned with the wall shear stress and the transverse component perpendicular to it is described in van den Berg [1973], van den Berg [1975], which accounts for streamwise and spanwise pressure gradients.
The paper is organized as follows. The theoretical background of boundary-layer theory, models for the total shear stress, scaling of the inner layer, and self-similarity is described in section 2. The database of turbulent boundary-layer flow experiments in APGs is presented in section 3. The methods used for the evaluation of the mean-velocity profiles are described in section 4. The results are presented in section 5. The correlations for the wall law in an APG are given in section 6. An attempt to discuss the issues of a local wall law, the moving-equilibrium concept, history effects, and effects of the measurement accuracy is given in section 7. The conclusions are given in section 8.
Finally, as implied in the title, the connection between the present analysis and RANS turbulence models is briefly described. A preliminary APG modification was presented for the SST k-ω model in Knopp [2016] and for the SSG/LRR-ω model in Knopp et al. [2022]. The idea is to use a model augmentation term in conjunction with a blending function. The augmentation term is added to the transport equation for the specific rate of turbulent dissipation ω. It is designed to obtain the assumed solution for the mean velocity and the turbulence quantities in the half-power law region. The blending function is used to activate the augmentation term only in the half-power law region. It has a value of unity in the half-power law region, and is zero in the log-law region and for $y > 0.2\delta$. It is based on the correlations that describe the regions of the log law and the half-power law as functions of y^+, Re_τ, Δp_s^+ and y/δ (see section 6). Addition-

ally, the calibration of the coefficient of the augmentation term depends on the empirical value found for the slope coefficient of the half-power law, denoted here by K. The value of K is determined from the experimental data in section 6.

Chapter 2

Boundary-Layer Theory

This section presents the theoretical results used for the design and the calibration of the wall law. The boundary-layer approximation is given in section 2.1. A local model for the total shear stress is described in section 2.2. The structure of the wall law is presented in section 2.3. A modified velocity scale for the inner layer is described in section 2.4. Some aspects for self-similarity of the mean-velocity profile are given in section 2.5.

2.1 Boundary-Layer Approximation

Two-dimensional, incompressible turbulent boundary-layer flow in a wall-fitted coordinate system with streamwise wall-parallel direction s, wall-normal direction y and corresponding velocity components U, V is assumed (see Hinze [1975])

$$\nu\frac{\partial^2 U}{\partial y^2} - \frac{\partial\overline{u'v'}}{\partial y} = \frac{1}{\rho}\frac{\mathrm{d}P_\mathrm{w}}{\mathrm{d}s} + U\frac{\partial U}{\partial s} + V\frac{\partial U}{\partial y} + \frac{\partial}{\partial s}\left(\overline{u'^2} - \overline{v'^2}\right) . \tag{2.1}$$

Here the relation $P(s,y) = P_\mathrm{w}(s) - \rho\,\overline{v'^2}(s,y)$ is used from the integration of the boundary-layer equation for V. The subscript w indicates values at $y = 0$. Integration of (2.1) from the wall to the wall-distance y gives the following relation for the total shear stress τ

$$\frac{\tau}{\rho} \equiv \nu\frac{\partial U}{\partial y} - \overline{u'v'} = \frac{\tau_w}{\rho} + \frac{1}{\rho}\frac{\mathrm{d}P_\mathrm{w}}{\mathrm{d}s}y + I_\mathrm{cu}(y) + I_\mathrm{cv}(y) + I_\mathrm{r}(y) \tag{2.2}$$

where τ_w denotes the wall shear stress and with the following notation

$$I_\mathrm{cu}(y) = \int_0^y U\frac{\partial U}{\partial s}\,\mathrm{d}\tilde{y}\,, \quad I_\mathrm{cv}(y) = \int_0^y V\frac{\partial U}{\partial \tilde{y}}\,\mathrm{d}\tilde{y}\,, \quad I_\mathrm{r}(y) = \int_0^y \frac{\partial}{\partial s}\left(\overline{u'^2} - \overline{v'^2}\right)\mathrm{d}\tilde{y} \tag{2.3}$$

for the integrated convective term and the Reynolds normal stress term.
Note that in the three-dimensional case, the direction s used in (1.2) is defined by the direction of the wall-parallel velocity as $y \to 0$ (being the direction of the skin friction vector).

2.2 A Local Model for the Total Shear Stress

The next step is to motivate local surface parameters to characterise the different terms in the mean momentum balance and hence the mean-velocity profile in the inner layer. A first-order local model for the total shear stress was proposed by Coles [1956] and Perry [1966]. It is based on the following ansatz for the mean-velocity profile in the inner layer

$$U(s,y) = u_\tau(s)\, f(y^+(s,y))\,, \quad y^+(s,y) = u_\tau(s) y/\nu\,. \tag{2.4}$$

As described in van den Berg [1973] and Knopp et al. [2015], the mean-inertia term can be written as

$$\int_0^y U\frac{\partial U}{\partial s}\,\mathrm{d}\tilde{y} + \int_0^y V\frac{\partial U}{\partial \tilde{y}}\,\mathrm{d}\tilde{y} = \nu\frac{\mathrm{d}u_\tau}{\mathrm{d}s}\int_0^{y^+} f^2\,\mathrm{d}\tilde{y}^+\,. \tag{2.5}$$

By substitution of (2.5) into (2.3) and neglecting the contribution of the Reynolds normal stress term $I_\mathrm{r}^+(y^+)$ in (2.3), the result for $\tau^+ = \tau/\tau_w$ is

$$\tau^+(y^+) = 1 + \Delta p_s^+ y^+ + \Delta u_{\tau,s}^+ I_1^+\,, \quad \Delta u_{\tau,s}^+ = \frac{\nu}{u_\tau^2}\frac{\mathrm{d}u_\tau}{\mathrm{d}s} \quad I_1^+ = \int_0^{y^+} f^2 \mathrm{d}\tilde{y}^+ \tag{2.6}$$

showing that the total shear stress in the inner layer not only depends on Δp_s^+ but also on the wall-shear-stress-gradient parameter $\Delta u_{\tau,s}^+$, which describes the local flow deceleration. The approximation to neglect $I_\mathrm{r}^+(y^+)$ if the flow is far from incipient separation is supported by the DLR/UniBw experiment II (see figures 7.1 and 7.2 in Knopp [2019]). Note that in the y^+-region where the mean-velocity profile follows the log law I_1^+ can be approximated by equation (8) in Galbraith et al. [1977]

$$\tau^+ = 1 + \Delta p_x^+ y^+ + \Delta u_{\tau,x}^+ \left[y^+\left(k_1\left(\log y^+\right)^2 + k_2\log(y^+) + k_3\right) + k_4\right] \tag{2.7}$$

for $y^+ > 30$ with constants $k_1, \ldots, k_4$ depending only on κ and B. The total shear stress is approximated by a linear relation in e.g. McDonald [1969]

$$\tau^+ = 1 + \alpha^+ y^+\,, \qquad \alpha^+ \equiv \lambda \Delta p_s^+\,, \tag{2.8}$$

where λ is a constant smaller than one, and $\alpha^+ \equiv \lambda\Delta p_s^+$ is called the effective pressure gradient. For flows in a mild adverse pressure gradient near equilibrium, $\lambda = 0.7$ was proposed in McDonald [1969], and from Perry et al. [1966] a value of 0.833 can be inferred at the outer edge of the logarithmic layer for the flows considered in their work. Similar values were found in Knopp et al. [2015]. The linear approximation (2.8) can be inferred from (2.7) for small values of $\Delta u_{\tau,s}^+$ and y^+.

A higher-order model for τ^+ can be obtained by extending (2.4), motivated by the dependence of f on Δp_s^+ in the half-power law

$$U(s,y) = u_\tau(s)\, f(y^+(s,y), \Delta p_s^+(s))\,, \quad y^+(s,y) = u_\tau(s) y/\nu \tag{2.9}$$

to account for higher-order effects on τ^+. The extended model for τ^+, which is described in detail in Knopp et al. [2015], includes the additional local flow parameter $\Delta^2 p_s^+$ which involves $\mathrm{d}^2P/\mathrm{d}s^2$. This higher-order local parameter will be used in the discussion of the conjecture of a local wall law in subsections 7.1 and 7.2. Note that, if the log law is unaltered, then the higher-order contribution is zero.

2.3 Log Law/Half-Power Law

For the mean-velocity profile in an adverse pressure gradient, a log-law/half-power-law structure is assumed, motivated by the findings described in the introduction

$$u^+ = \begin{cases} u^+_{\log} & \text{if} \quad y^+ \in (y^+_{\log,\min},\, y^+_{\log,\max}) \\ u^+_{\mathrm{sqrt}} & \text{if} \quad y^+ \in (y^+_{\mathrm{sqrt},\min},\, y^+_{\mathrm{sqrt},\max}) \end{cases} \tag{2.10}$$

with the log law

$$u^+_{\log} = \frac{1}{\kappa}\log(y^+) + B \tag{2.11}$$

and the extended wall law (involving the parameter α^+ defined in (2.8))

$$u^+_{\mathrm{sqrt}} = \frac{1}{K}\left[2\left((1+\alpha^+ y^+)^{\frac{1}{2}} - 1\right) + \log(y^+) + 2\log\left(\frac{2}{(1+\alpha^+ y^+)^{\frac{1}{2}}+1}\right)\right] + B_{\mathrm{o}}\,. \tag{2.12}$$

The parameter α^+ defined in (2.8). The designation "half-power law" is used loosely for the extended wall law.
Note that there is an intermediate region in which neither the log law nor the half-power law describes the mean velocity. The important parameters for the calibration are $y^+_{\log,\max}$ and $y^+_{\mathrm{sqrt},\min}$. They describe the reduction of the log-law region, and are supposed to depend, among other effects, on the pressure gradient and on the Reynolds number. They will be calibrated using the database. The half-power law is assumed to extend up to the outer edge of the inner layer. The value for κ is assumed to be constant with $\kappa = 0.41$, and K will be studied in section 6.4. The value of $y^+_{\log,\min}$ is expected to depend on the Reynolds number and possibly on the pressure gradient, but is not considered in this work. Note the alternative form of the half-power law by Stratford [1959] for zero-skin-friction flows

$$U(y) = \frac{2}{K}\left(\frac{1}{\rho}\frac{\mathrm{d}P}{\mathrm{d}s}\right)^{1/2} y^{1/2} + C \tag{2.13}$$

which was recently confirmed by the DNS of Coleman et al. [2017].

2.4 A Velocity Scale for the Inner Layer

The classical velocity scale for the inner layer u_τ leads to well-known issues as the flow approaches separation. As $u_\tau \to 0$, the profile u^+ versus y^+ is not defined. Moreover, boundary-layer parameters involving u_τ, e.g.,

$$Re_\tau \equiv \delta^+ = \frac{\delta u_\tau}{\nu}\,, \qquad \beta_{\mathrm{RC}} = \frac{\delta^*}{\rho u_\tau^2}\frac{\mathrm{d}P_w}{\mathrm{d}s} \tag{2.14}$$

and Δp_s^+, are approaching zero or infinity. In particular, the Reynolds number δ^+ is found to give decreasing values as the flow approaches separation, whereas Re_θ and Re^*_δ are increasing, and Δp_s^+ and β_{RC} can reach high values mainly

due to the small values of u_τ.
A modified velocity scale for the inner layer was devised in Nickels [2004] as a part of an analytical model for the mean velocity depending on the local value of Δp_s^+. It involves the quantity y_c^+, which is associated with the thickness of the viscous sublayer and related to a critical value of the local Reynolds number based on the total shear stress (cf. (2.6), neglecting the convective term)

$$Re_c = \frac{u_\mathrm{T} y_c}{\nu}, \qquad u_\mathrm{T} = \left(\frac{\tau|_{y=y_c}}{\rho} \right)^{1/2}, \qquad \tau^+|_{y=y_c} = 1 + \Delta p_s^+ y_c^+ \,. \quad (2.15)$$

The assumption that Re_c has a universal value for all wall-bounded flows ($Re_c = 12$) leads to a cubic equation for y_c^+, which can be interpreted as the critical value above which the viscous sublayer becomes unstable,

$$\Delta p_s^+ \left(y_c^+\right)^3 + \left(y_c^+\right)^2 - Re_c^2 = 0 \,. \quad (2.16)$$

The only free parameter of this model is Re_c, for which the value $Re_c = 12$ was chosen from zero-pressure-gradient data. The physically relevant solution for y_c is the smallest positive root of (2.16).
The exact solution for y_c follows from the formula by del Ferro, Tartaglia, and Cardano (see Nickels [2004]). For large Δp_s^+ this solution may be approximated by

$$y_c^+ = \frac{Re_c^{2/3} (\Delta p_s^+)^{2/3} - \frac{1}{3}}{\Delta p_s^+} \quad (2.17)$$

(see also eq. (10.1) in Nickels [2004]). As $u_\tau \to 0$ (and $\Delta p_s^+ \to \infty$)

$$u_\mathrm{T} = u_\tau (1 + \Delta p_s^+ y_c^+)^{1/2} \to Re_c^{1/3} u_p \,, \quad (2.18)$$

i.e., u_T converges to the non-zero value $Re_c^{1/3} u_p$. Here $u_p = |\nu/\rho \mathrm{d}P_\mathrm{w}/\mathrm{d}s|^{1/3}$ is the so-called pressure-viscosity velocity by Stratford [1959] and Mellor [1966] with $\Delta p_s^+ = (u_p/u_\tau)^3$.
For $0 < \Delta p_s^+ < 0.1$, the analytical solution of (2.16) can be approximated by

$$y_c^+ \approx Re_c (1 + y_{c,0}^+ \Delta p_s^+)^{-1/3} \,, \qquad y_{c,0}^+ = 16 \,. \quad (2.19)$$

Figure 2.1 provides some illustration for y_c^+ (left) and for u_T/u_τ (right). Note that, alternatively, the solution of (2.16) can be computed using Newton's method, and can be approximated by the maximum of (2.17), (2.19). The above model could require modification for large values of Δp_s^+. A first issue is that the mean-inertia term can become important and needs to be accounted for in the approximation of τ^+ in (2.15). A second issue concerns possible effects of incipient separation and instantaneous reverse flow.

2.5 Self-Similarity

The existence of a wall law, which depends only on local flow parameters at the corresponding nearest wall point, is related to the question of self-similarity of the mean-velocity profile in the inner layer. Self-similarity is associated with a

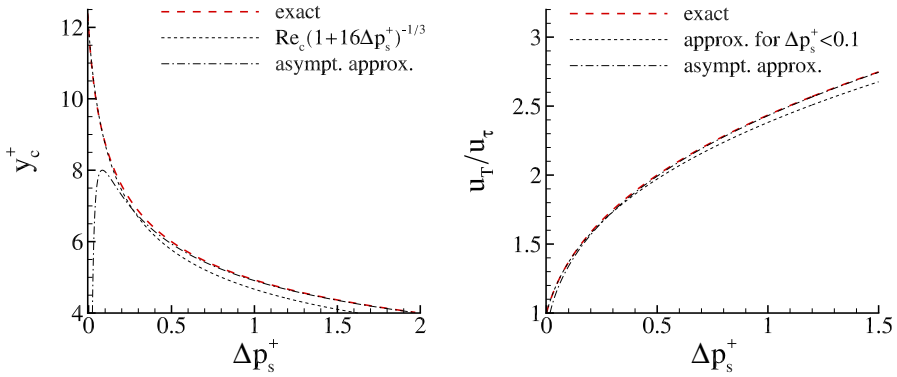

Figure 2.1: Behaviour of y_c^+ (left) from (2.16), (2.17), (2.19) and modified velocity scale u_T (right).

state of a dynamic equilibrium of (2.1) in the sense that the streamwise variation of the relative magnitude of the different terms of the mean momentum balance (pressure gradient, mean inertia, viscous stresses and Reynolds stresses) is negligible with respect to other terms (see Gungor et al. [2016], Rotta [1950], and Clauser [1954]). The classical approach is to seek a similarity solution of the form

$$U(s,y) = U_e(s) f'(\eta)\,, \quad \overline{u'v'} = u_t^2(s)\, t(\eta)\,, \quad \eta(s,y) = \frac{y}{\delta(s)}\,. \tag{2.20}$$

Note that the choice for u_t for a self-similar scaling of the Reynolds stresses is still open in the literature (see Elsberry et al. [2000]). Then consider (2.1), with the streamwise gradients of the Reynolds stresses being neglected. They are included in the study by Elsberry et al. [2000], Kitsios et al. [2017]. Substitution of (2.20) yields (see e.g. Dixit and Ramesh [2008])

$$-\frac{\delta U_e}{\nu}\frac{\mathrm{d}\delta}{\mathrm{d}s}\left[f''f\right] + \frac{\delta^2}{\nu}\frac{\mathrm{d}U_e}{\mathrm{d}s}\left[(f')^2 - f''f - 1\right] = f''' + \frac{U_e\delta}{\nu}\left(\frac{u_t}{U_e}\right)^2 t'\,. \tag{2.21}$$

A similarity solution exists only if the coefficients are independent of s

$$\beta_1 \equiv \frac{\delta U_e}{\nu}\frac{\mathrm{d}\delta}{\mathrm{d}s} = \mathrm{const}\,, \quad \beta_H \equiv \frac{\delta^2}{\nu}\frac{\mathrm{d}U_e}{\mathrm{d}s} = \mathrm{const}\,, \quad \beta_3 \equiv \frac{U_e\delta}{\nu}\left(\frac{u_t}{U_e}\right)^2 = \mathrm{const}\,. \tag{2.22}$$

If all conditions are met, then the flow is self-similar in the inner and outer layer, whereas, if only β_H is independent of s, then the flow is self-similar only in the outer part, as described in Kitsios et al. [2017], Vila et al. [2020]. Note that β_H is the Hartree parameter in the laminar case. It can be written as

$$\beta_\mathrm{H} = \frac{\delta^2}{\nu}\frac{\mathrm{d}U_e}{\mathrm{d}s} = -\Delta p_s^+\, Re_\tau^2 \left(\frac{u_\tau}{U_e}\right)\,. \tag{2.23}$$

and alternatively in the form $\beta_\mathrm{H} = -\beta_\mathrm{RC}\, Re_\tau^2\, Re_{\delta^*}^{-1}$. Traditionally, β_RC is seen to be the governing parameter of the similarity solution, although there are

two parameters arising for the mean-inertia and for the pressure-gradient terms and a third parameter for the Reynolds shear stress, in agreement with the findings of (2.6). Note that the additional assumption of a power law behaviour of $U_e(s) \sim s^m$ and of $\delta(s)$ leads to the relation $\beta_1 = 1 - \beta_H$. An additional constraint is that $Re_\delta = U_e\delta/\nu$ and u_τ/U_e are constant in streamwise direction (involving the choice $u_t = u_\tau$). The latter condition implies that Δp_s^+ and $\Delta u_{\tau,s}^+$ are in a constant ratio, which can be seen from the relation

$$\Delta u_{\tau,s}^+ = -\frac{u_\tau^2}{U_e^2}\Delta p_s^+ + \frac{\nu U_e}{u_\tau^2}\frac{\mathrm{d}}{\mathrm{d}s}\left(\frac{u_\tau}{U_e}\right) . \tag{2.24}$$

This implies a similarity solution for τ^+ in (2.6) for y^+ large enough so that viscous effects lose leading order influence. The condition $\mathrm{d}Re_\delta/\mathrm{d}s = 0$ is rather restrictive, and implies that $\beta_1 = -\beta_H$. The resulting equation for (2.21) has a non-trivial solution only for sink flows, i.e., in a favourable pressure gradient (FPG), in the case of a smooth wall.

Chapter 3

Database

A database study was performed to account for the variety of turbulent boundary-layer flows in an APG and the richness of the parameter space. Based on the assumption that an asymptotic structure of the mean velocity profile arises only for sufficiently large Re, the focus is on mean-velocity profiles from experiments with $Re_\theta > 8000$. Moreover, two data sets from experiments and DNS for small Re are included to assess the validity of the wall law for small Re.

3.1 Experimental Data

The database covers the famous test-case collection Coles and Hirst [1969]. published at the 1968 Stanford conference on the computation of turbulent boundary layers. Additionally, the more recent experiments by Samuel and Joubert [1974], Skare and Krogstad [1994], Marusic and Perry [1995], and Romero et al. [2022] are used. Two joint DLR/UniBw turbulent boundary-layer experiments designed to yield data for $\Delta p_s^+ > 0.01$ are also included. The database is restricted to boundary layers, i.e., Couette-Poiseuille flows are not considered. For the data in the collection by Coles and Hirst [1969], their identifiers (IDENTs, abbreviated IDs) are used to denote the flows and the streamwise positions. The test-cases used from the 1968 Stanford data collection are given in table 4.1-4.2. The flows by Clauser and by Bradshaw are equilibrium flows. The equilibrium flows by Clauser Clauser [1954] in a mild APG (2200) and in a moderate APG (2300) are used. From the work by Bradshaw, the equilibrium flows in a mild APG (2500) Bradshaw [1966] and in a moderate APG (2600) Bradshaw [1965] by Bradshaw & Ferriss are used. Regarding the streamwise evolving flows, the data by Ludwieg & Tillmann, Perry, Schubauer & Klebanoff, Bradshaw, and Schubauer & Spangenberg are considered. The turbulent boundary-layer flows by Ludwieg & Tillmann Ludwieg and Tillmann [1949] are in a mild (1100) and in a strong (1200) APG. The turbulent boundary layer by Perry Perry [1966] is in a decreasing APG and at large values for Re_θ and β_{RC}. High values for Re, β_{RC} and Δp_s^+ were also reached for the boundary layer on a large airfoil-like body (2100) by Schubauer & Klebanoff Schubauer and Klebanoff [1950]. The flow 3300 by Bradshaw Bradshaw [1967] develops from initially constant pressure into an equilibrium flow in a moderate APG. From the work by Schubauer & Spangenberg Schubauer and Sprangenberg [1960], flow B in a moderate APG

(4500) and flow E in a mild APG (4800) are used.
Moreover, some more recent experiments are used (see table 4.1-4.2). The flow by Samuel & Joubert is in an increasing APG to study the effect of $\mathrm{d}^2P/\mathrm{d}s^2$. Samuel & Joubert Samuel and Joubert [1974] studied a turbulent boundary-layer flow in an increasing APG with both $\mathrm{d}P/\mathrm{d}s$ and $\mathrm{d}^2P/\mathrm{d}s^2$. The flow by Marusic & Perry Marusic and Perry [1995] was at Re_θ up to 19200. The equilibrium flow by Skare & Krogstad Skare and Krogstad [1994] reached high values for both $\Delta p_s^+ = 0.012$ and Re_θ up to 54300. In the experiment at the University of New Hampshire (UNH) by the group of Klewicki Romero et al. [2022], the APG was mild and $20600 < Re_\theta < 26500$.
Moreover, two joint DLR/UniBw turbulent boundary-layer experiments are considered. They were designed to study the mean-velocity profile in the inner layer at large values of Δp_s^+ and Re_θ. The DLR/UniBw experiment I was at an inflow velocity U_∞ up to 12 m/s, and in the APG region values of Δp_s^+ up to 0.045 and Re_θ up to 18000 were obtained (see Knopp et al. [2015]). The DLR/UniBw experiment II was at inflow velocities 23 m/s and 36 m/s, leading to $\Delta p_s^+ > 0.01$ and Re_θ up to 60000 in the APG region (see Knopp et al. [2021]).
Two data sets at small Re are included. For the wind tunnel experiment by Nagano et al. Nagano et al. [1991] the mean-velocity profiles are for $481 \leq Re_\tau \leq 639$, $1290 \leq Re_\theta \leq 3350$ and $0.009 \leq \Delta p_s^+ \leq 0.025$. For the DNS of a turbulent boundary layer with separation and reattachment by Coleman et al. Coleman et al. [2018], Re_τ is up to 880 and $2000 \leq Re_\theta \leq 6400$ in the APG region, and Δp_s^+ is increasing from 0.001 to values exceeding 1 as the flow is approaching separation. Note that the low-Re data are used only in section 7.3 to assess the validity of the wall law for small Re. The test cases and their acronyms are summarised in table 4.1-4.2.

3.2 Boundary-Layer Characterisation

The characterisation of turbulent boundary-layer flows in adverse pressure gradients using suitable boundary-layer parameters is still open (cf. Vila et al. [2017]). The parameter space is much wider than for the zero-pressure-gradient case. Figure 3.1 (left) shows β_{RC} versus Re_θ. Each symbol corresponds to a mean-velocity profile. The number of data points for $Re_\theta > 30000$ is small. The strength of the APG felt in the inner layer can be described by Δp_s^+. The values of Δp_s^+ plotted against Re_τ are shown in figure 3.1 (right). Only in a small number of experiments are values of $\Delta p_s^+ > 0.02$ reached.

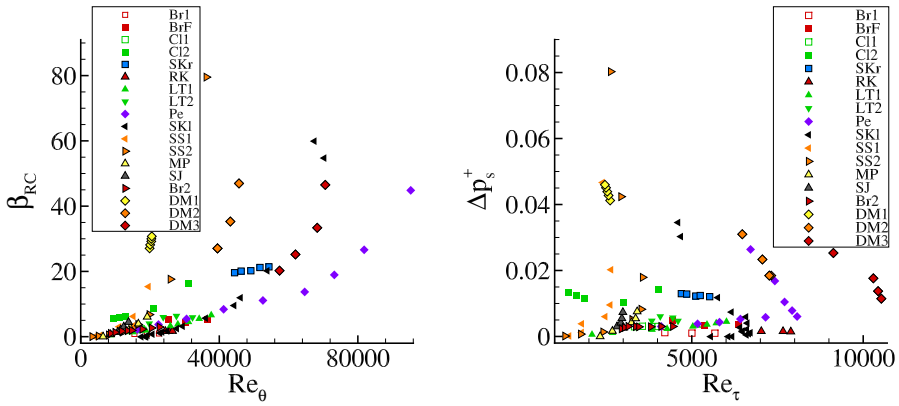

Figure 3.1: Characterisation of the turbulent boundary-layer flows in the database.

Chapter 4

Methods for Data Evaluation

This section describes the methods used for the evaluation of the data. The methods to determine the friction velocity u_τ and the boundary-layer thickness δ are described in section 4.1. Section 4.2 describes the methods used to identify the regions of the log law and the half-power law. Finally, the assessment of the data in the region of the half-power law is described in section 4.3.

4.1 Fit to the Law-of-the-Wall/Law-of-the-Wake

In the collection by Coles & Hirst Coles and Hirst [1969], the boundary-layer thickness δ, the wake factor Π, and the friction velocity u_τ were determined such that the root-mean-square (r.m.s.) deviation of the data from the law-of-the-wall/law-of-the-wake

$$u^+ = \frac{1}{\kappa}\log(y^+) + B + \frac{2\Pi}{\kappa}\left(\sin\left(\frac{\pi\eta}{2}\right)\right)^2, \quad \eta = \frac{y}{\delta} \tag{4.1}$$

is minimised. The values $\kappa = 0.41$ and $B = 5.0$ by Coles & Hirst were used for all cases throughout this work, except for the experiments by DLR/UniBw experiments and by UNH and the two flows at small Re, for which almost direct values for u_τ are provided. A similar evaluation as in Coles and Hirst [1969] was provided for the flows by Skare and Krogstad [1994] and Marusic and Perry [1995]. Note that the recently proposed methods to determine the boundary-layer thickness by Coleman et al. [2018] and Vinuesa et al. [2016] are not used in the present method, as they require additional data which are not available for most of the old data sets in the database.
The first step was a review of the values reported for δ, Π, and u_τ. First, the mean-velocity profiles were plotted in viscous units and compared with the log law to assess u_τ. The original values for u_τ could be supported and were used for the data analysis. This concurs with the result by Patel [1965], reporting an uncertainty within 6% for $\Delta p_s^+ < 0.015$ for the Preston tube. This was seen to be acceptable, given the different sources of uncertainties.
The next step was to review the values for δ. The aim was to ensure comparable and consistent values for δ among all test cases. The mean-velocity profiles

in viscous units were compared with (4.1) in the law-of-the-wake region, and overall, the values reported for δ and Π were found to give a good agreement. For some data sets, minor adjustments in δ by visual inspection were applied to obtain a similar matching between the experimental data and (4.1) near the boundary-layer edge. This is summarised in table 4.1-4.2, which is explained at the end of this section.

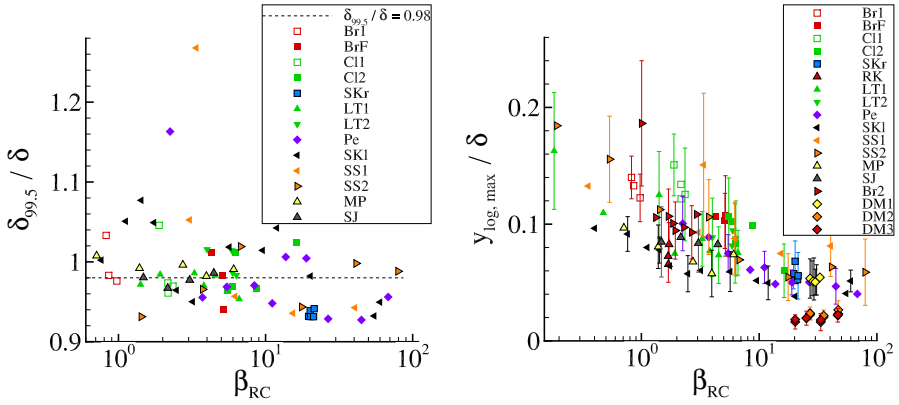

Figure 4.1: Comparison of $\delta_{99.5}$ and δ (left) and $y^+_{\mathrm{log,max}}/\delta$ versus β_{RC} (right).

The evaluation of u_τ and δ was different for the UNH experiment Romero et al. [2022] and for the DLR/UniBw experiments Knopp et al. [2015] and Knopp et al. [2021]. For the UNH flow, the values for u_τ were determined by matching the hot-wire data for the mean velocity with the LES mean-velocity profiles by Bobke et al. [2017] for $y^+ < 40$. Note that the values for u_τ were confirmed by the author using the Clauser-chart method (CCM) with $\kappa = 0.41$ and $B = 5.0$ in the region where the mean velocity follows the log law. The relative deviation in u_τ was found to be below 1.5%. Regarding the boundary-layer thickness, the values by Romero et al. [2022] are used, which were determined using an indirect method involving the profile for $\overline{u'^2}$ (see Romero et al. [2022]). The values were supported by the evaluation of $\delta_{99.5}$ by the author, although, following Romero et al. [2022], the measurement resolution near the boundary-layer edge was a little bit too coarse for the evaluation.
For the DLR/UniBw experiment II at $x = 9.944\,\mathrm{m}$, u_τ was determined using oil film interferometry (OFI) and from the 2D μPTV and 3D LPT data using an (almost) direct method based on a least-squares fit of the data with the mean-velocity profile by Nickels for $y^+ < 20$ (see Knopp et al. [2021]). For the other positions, u_τ was determined from the 2D2C PIV data using the standard CCM. For the boundary-layer thickness $\delta_{99.5}$ was used, as a close matching with (4.1) could not be obtained, possibly due to history effects. Note that for all flows, $\delta_{99.5}$ was found to be in close agreement with δ (see figure 4.1 (left)).
The data evaluation is summarised in table 4.1-4.2. The fourth column gives the source for the value used for u_τ. In the fifth column, the method used to determine the boundary-layer thickness is specified. Here δ denotes the approach by Coles and Hirst [1969]. The values used for δ are given in the sixth column. These are mainly the values by Coles and Hirst [1969], although the recomputed values (denoted by re) are used for some of the streamwise evolving flows. For

the flow by Marusic & Perry, the recomputed values are used. For the flow by Samuel & Joubert, δ was determined by the author. The next column gives the maximum deviation for δ in percent between the original value and the recomputed value. The number in brackets gives the number of mean-velocity profiles for which the deviation is greater than 1%. This shows that the deviation between the values by Coles and Hirst [1969] and the recomputed values is small compared to the other sources of uncertainties. Note that for the flow by Marusic & Perry, the deviation between the original values for δ and the recomputed values was smaller than 8% for the last four profiles in the region of the strongest APG. The next column specifies the values for κ and B used to determine the extent of the log-law region $y^+_{\mathrm{log,max}}$ (see the next subsection). The log-law with $\kappa = 0.41$ and $B = 5.0$ by Coles & Hirst is denoted by "Coles and Hirst [1969]", whereas "fit" indicates that κ and B are fitted to the mean-velocity profile, which is described in detail in the next section. The last column summarises the assessment for the calibration of the half-power law using the criteria C1 - C4 described in subsection 4.3.

Table 4.1: Summary of the data evaluation and the acronyms used in the figure legends.

Acro-nym	Author(s)	Ref.	Val. for u_τ
Br1	Bradshaw, mild	Bradshaw [1966]	Coles and Hirst [1969]
BrF	Bradshaw & Ferriss	Bradshaw [1965]	Coles and Hirst [1969]
Cl1	Clauser, mild	Clauser [1954]	Coles and Hirst [1969]
Cl2	Clauser, moderate	Clauser [1954]	Coles and Hirst [1969]
LT1	Ludwieg & Till., mild	Ludwieg and Tillmann [1949]	Coles and Hirst [1969]
LT2	Ludwieg & Till., strong	Ludwieg and Tillmann [1949]	Coles and Hirst [1969]
Pe	Perry	Perry [1966]	Coles and Hirst [1969]
SKl	Schubauer & Klebanoff	Schubauer and Klebanoff [1950]	Coles and Hirst [1969]
SS1	Schubauer & Spang., B	Schubauer and Sprangenberg [1960]	Coles and Hirst [1969]
SS2	Schubauer & Spang., E	Schubauer and Sprangenberg [1960]	Coles and Hirst [1969]
Br2	Bradshaw	Bradshaw [1967]	Coles and Hirst [1969]
SJ	Samuel & Joubert	Samuel and Joubert [1974]	Samuel and Joubert [1974]
MP	Marusic & Perry	Marusic and Perry [1995]	Marusic and Perry [1995]
SKr	Skare & Krogstad	Skare and Krogstad [1994]	Skare and Krogstad [1994]
RK	Romero & Klew. (UNH)	Romero et al. [2022]	Romero et al. [2022]
DM1	DLR/UniBw I	Knopp et al. [2015]	Knopp et al. [2015]
DM2	DLR/UniBw II 23 m/s	Knopp et al. [2021]	Knopp et al. [2021]
DM3	DLR/UniBw II 36 m/s	Knopp et al. [2021]	Knopp et al. [2021]
Na	Nagano et al.	Nagano et al. [1991]	Nagano et al. [1991]
CSR	Coleman et al., case C	Coleman et al. [2018]	Coleman et al. [2018]

Table 4.2: Summary of the data evaluation and the acronyms used in the figure legends.

Acro-nym	Val. for δ	$\Delta\delta_{\max}$[2] for δ	κ, (n)[3]	Criteria B	calibrat.
Br1	δ	Coles and Hirst [1969]	3.4(3)	0.41, 5.0	− − −+
BrF	δ	Coles and Hirst [1969]	2.5(3)	0.41, 5.0	− − ++
Cl1	δ	Coles and Hirst [1969]	2.6(1)	0.41, 5.0	− + −+
Cl2	δ	Coles and Hirst [1969]	1.1(1)	0.41, 5.0	+ − ++
LT1	δ	re	2.5(2)	0.41, 5.0	+ + ++
LT2	δ	re	0.3(0)	0.41, 5.0	− − ++
Pe	δ	re	2.2(2)	0.41, 5.0	+ + +−
SKl	δ	re	1.5(2)	0.41, 5.0	+ + ++
SS1	δ	Coles and Hirst [1969]	0.2(0)	0.41, 5.0	− − ++
SS2	δ	Coles and Hirst [1969]	0.1(0)	0.41, 5.0	− − ++
Br2	δ	Coles and Hirst [1969]	5.0(2)	0.41, 5.0	− − −+
SJ	δ	re	-	0.41, 5.0	+ + ++
MP	δ	re	15.5(6)	0.41, 5.0	+ + ++
SKr	δ	Skare and Krogstad [1994]	-	0.41, 5.0	+ + ++
RK	Romero	Romero et al. [2022]	-	fit	+ − −+
DM1	$\delta_{99.5}$	Knopp et al. [2015]	-	fit	+ + +−
DM2	$\delta_{99.5}$	Knopp et al. [2021]	-	fit	+ + +−
DM3	$\delta_{99.5}$	Knopp et al. [2021]	-	fit	+ + +−
Na	$\delta_{99.5}$	re	-	fit	
CSR	$\tilde{\delta}_{99.5}$[1]	Coleman et al. [2018]	-	fit	

4.2 Identification of Log Law and Half-Power Law

The next step was the identification of the log-law and the half-power law region. The log-law region is referred to as the region in which the mean-velocity profile can be fitted by a log law. The half-power law region is defined analogously. The notation introduced in section 2.3 is used. For illustration, figure 4.2 shows the mean-velocity profiles for the flow by Ludwieg & Tillmann (1108) at $\Delta p_s^+ = 3.05 \times 10^{-3}$, $Re_\theta = 25870$ and $Re_\tau = 5031$ (left) and for the flow by Samuel & Joubert at $\Delta p_s^+ = 0.00735$, $Re_\theta = 13804$ and $Re_\tau = 2990$ (right).
For the evaluation of $y^+_{\log,\max}$, for each mean-velocity profile, the maximum wall-distance was determined up to which the experimental data for u^+ follow the log law (2.11). The method to determine $y^+_{\log,\max}$ was based on visual inspection and the determination of the y^+-position, where a best-approximation polynomial through the data points above the log-law region smoothly joins the log law. The results for $y^+_{\log,\max}$ are plotted against β_{RC} in figure 4.1 (right). Here $\kappa = 0.41$ and $B = 5.0$ was used in (2.11) for all flows, except for the flows by DLR/UniBw and UNH. Note that the influence of using a fitted value for κ versus a constant value is discussed below for the DLR/UniBw experiment and in section 7.3.
For the flows by DLR/UniBw and UNH, u_τ was determined independently of the assumption of the log law. The profiles for u^+ show a departure from the

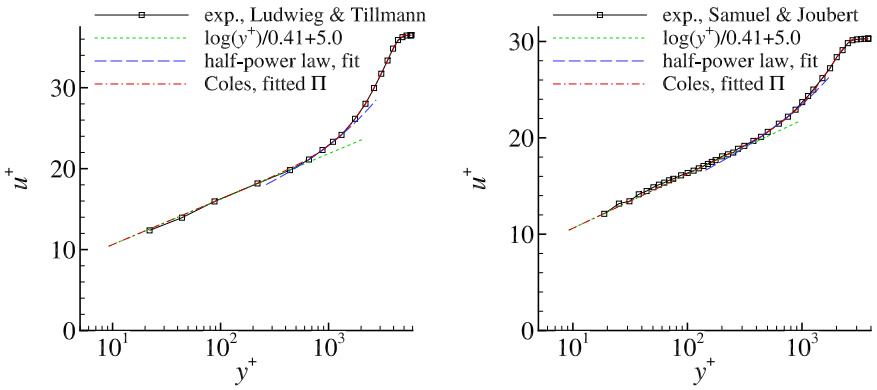

Figure 4.2: Left: Ludwieg & Tillmann, mild APG (1108) at $\Delta p_s^+ = 3.05 \times 10^{-3}$ and $Re_\tau = 5031$. Right: Samuel & Joubert, mild APG at $\Delta p_s^+ = 7.35 \times 10^{-3}$ and $Re_\tau = 2990$.

log law with $\kappa = 0.41$ and $B = 5.0$. An iterative method was used to determine the fitted values for κ and B and $y^+_{\log,\max}$ simultaneously under the constraint to minimise the least-squares error in the y^+-interval used for the fit, which was successively adjusted.

For the DLR/UniBw experiment, a study was made to assess the sensitivity of $y^+_{\log,\max}$ on details of the method used. The details are given in appendix B. The main conclusion is that the sensitivity of $y^+_{\log,\max}$ on details of the evaluation is small for the DLR/UniBw flow compared to the uncertainties of the older flows in the data base (see section 6.5).

The outer edge of the half-power law is assumed to extend up to $y = 0.2\delta$. The motivation for this assumption is the observation that the half-power law, if fitted up to $y = 0.15\delta$, describes the mean-velocity profile even up to $y = 0.2\delta$. The choice of $y = 0.2\delta$ has the advantage of increasing the number of data points for the half-power law fit compared to $y = 0.15\delta$.

The inner edge of the half-power law, denoted by $y^+_{\mathrm{sqrt,min}}$, is determined iteratively. In the first step, the two data points below and above $y = 0.15\delta$ are chosen and a preliminary fit is computed. Then this stencil is extended successively above and below $y = 0.15\delta$. The points with the smallest y^+ value are removed if such improves the overall fit; alternatively additional points are included successively if they are in agreement with the fit. For the final evaluation of the half-power law and after a comparison among all test cases, the outer edge is set to the constant value $y = 0.21\delta$. For the inner edge, the value determined by the iterative method described above is employed. The results are shown in figure 4.3. In case the above method does not identify two points for the half-power law fit below $y = 0.21\delta$, the outer edge is increased, but these data sets are then used with special care (see criterion C1 in section 4.3). Such can concern data sets whose log-law region is thick and extends to $y = 0.15\delta$.

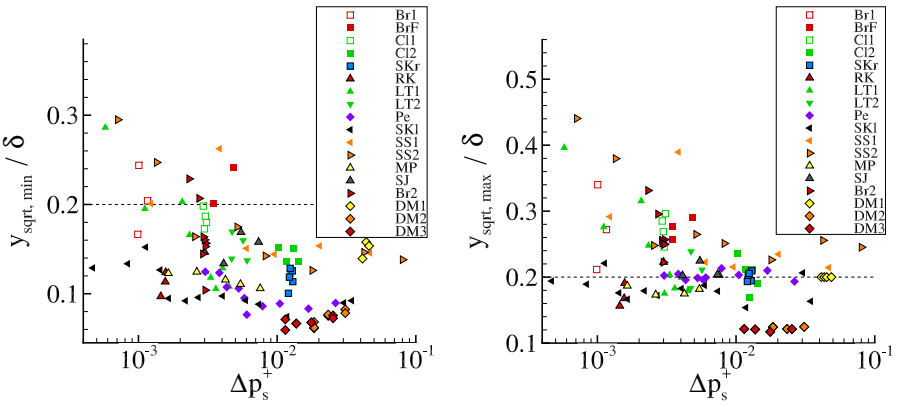

Figure 4.3: Inner edge (left) and outer edge (right) used for the fit to the half-power law.

4.3 Data Assessment for the Half-Power Law Region

For the calibration of the half-power law, the individual mean-velocity profiles need to be assessed, so that only the suitable ones are considered for the calibration. The number of data points in the half-power law region N_{sqrt} is an important quantity for the assessment, and is shown in figure 4.4 (left). This number can become large if Re_θ is large, if $y^+_{\mathrm{sqrt,min}}$ is significantly smaller than $0.15\delta^+$, or if the wall-normal spacing between adjacent data points Δy^+ is small. The largest values for N_{sqrt} are reached for the DLR/UniBw experiment II, exceeding 80 for the 2D2C PIV measurements and 250 for the 3D LPT measurement technique. For some mean-velocity profiles, the number of data points for the half-power law fit is only two. This small number can be due to a large spacing Δy^+ in conjunction with a thin half-power law region, or to the Reynolds number being insufficiently large. Interestingly, the half-power law fit is found to give a reasonable description even for these mean-velocity profiles. These profiles are considered with special care (see criterion C2 below) for the calibration of the wall law in sections 5 and 6.

A theoretical criterion for a half-power law in the form (2.13) was proposed by Yaglom [1979]. Based on the three length scales $\delta_\nu = \nu/u_\tau$, $\delta_p = \rho u_\tau^2/(\mathrm{d}P/\mathrm{d}s)$, and δ, the criterion can be written in the form $\delta_\nu \ll \delta_p \ll \delta$ (cf. Kader and Yaglom [1978], Yaglom [1979]), or alternatively in the form $\Delta p_s^+ \ll 1$ and $\delta^+ \Delta p_s^+ \gg 1$ (see Alving and Fernholz [1995]). The values of $\delta^+ \Delta p_s^+$ versus Δp_s^+ are shown in figure 4.4 (right) for the mean-velocity profiles in the database. From figure 4.4 (right) the downstream profiles of most data sets are meeting the criterion $\delta^+ \Delta p_s^+ > 15$ (see criterion C3 below), albeit a value of several tens is not considered to be very high by Yaglom [1979]. However, $\delta^+ \Delta p_s^+ > 100$ is reached only for a few mean-velocity profiles.

To summarise: for the assessment of the half-power law region, the following criteria are used:

- C1: Two data points in the half-power law region below $y/\delta = 0.21$ and $y_{\mathrm{sqrt,max}}/\delta \leq 0.21$ in figure 4.3 (right);

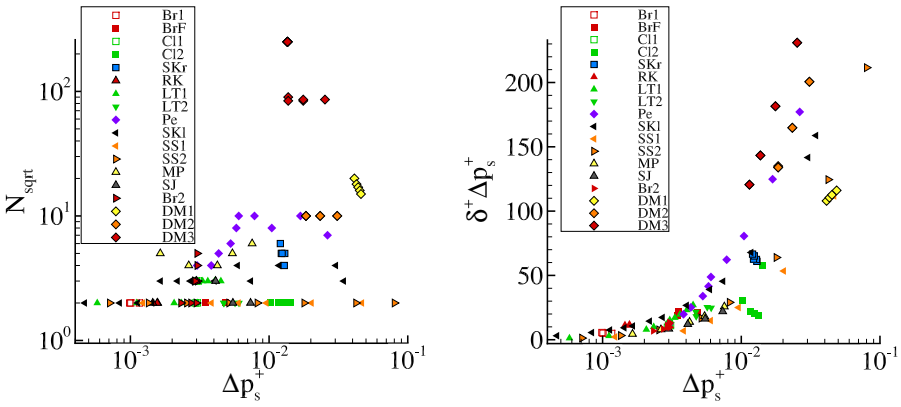

Figure 4.4: Number of data points N_{sqrt} in the half-power law region (left) and $\delta^+\Delta p_s^+$ versus Δp_s^+ (right).

- C2: $N_{\mathrm{sqrt}} \geq 3$ for most of the mean-velocity profiles (see figure 4.4 (left));
- C3: $\delta^+\Delta p_s^+ > 15$ for at least two mean-velocity profiles (see figure 4.4 (right));
- C4: No significant history effects in the APG region.

The assessment of these criteria is given in the last column of table 4.2. An additional minor criterion is the smoothness of the data, i.e., the spreading (or wiggles) of the data points around a smooth fit through the data points should be small. The calibration of the half-power law relies mainly on the data sets that satisfy all criteria. These are the flows by Perry, Skare & Krogstad, Schubauer & Klebanoff, Ludwieg & Tillmann (mild), Marusic & Perry, and Samuel & Joubert. The mean-velocity profiles by Perry, Skare & Krogstad, and Schubauer & Klebanoff are at a high Re, exhibit a relatively thick half-power law region and match all criteria C1 - C4. Among them, the lowest number of data points is for the case by Schubauer & Klebanoff, being only between three and five due to the large Δy^+-spacing. Note that some of the mean-velocity profiles by Perry, by Schubauer & Klebanoff, and by Skare & Krogstad show some wiggles. For the experiments by Marusic & Perry and by Ludwieg & Tillmann, the region identified for a half-power law fit has a significantly large extent, despite the moderately large Re.
Some of the flows are not considered for the final calibration of the half-power law (see table 4.1-4.2), violating already criteria C1 and C2. An additional difficulty is caused by the substantial wiggles in the data observed for the flows by Clauser and by Schubauer & Spangenberg. Nevertheless, these flows are useful to assess the calibration found for the more suitable data sets.
An important conclusion is the difficulty in assessing the half-power law for flows in mild and moderate APGs for the present database. At small and moderate Δp_s^+-values, high values of Re are needed to obtain a significant extent of the half-power law region given the criterion C3. Moreover, a high spatial resolution is needed to achieve a sufficiently large number of data points in the half-power law region. New experiments could shed more light on this issue.

Chapter 5

Results and Analysis

This section describes the results of the data evaluation and their analysis. The log-law/half-power-law fit for a variety of mean-velocity profiles of the database is illustrated in section 5.1. The robustness of the log law and the reduction of the extent of the log-law region in an APG are described in section 5.2.

5.1 Mean-Velocity Profiles

This section illustrates the wall law and the results of the fitting method described in section 4. First, two examples at moderately large values of Δp_s^+ are shown. The mean-velocity profile for the flow by Marusic & Perry Marusic and Perry [1995] at $x = 3.08\,\mathrm{m}$, $\Delta p_s^+ = 7.55 \times 10^{-3}$ and at moderately large $Re_\theta = 19188$ and $Re_\tau = 3406$ is shown in figure 5.1 (left). The profile for the flow by Perry at $\Delta p_s^+ = 7.85 \times 10^{-3}$ and high values of $Re_\theta = 73201$ and $Re_\tau = 7926$ (ID 2907) is given in figure 5.1 (right). Subsequently, profiles at

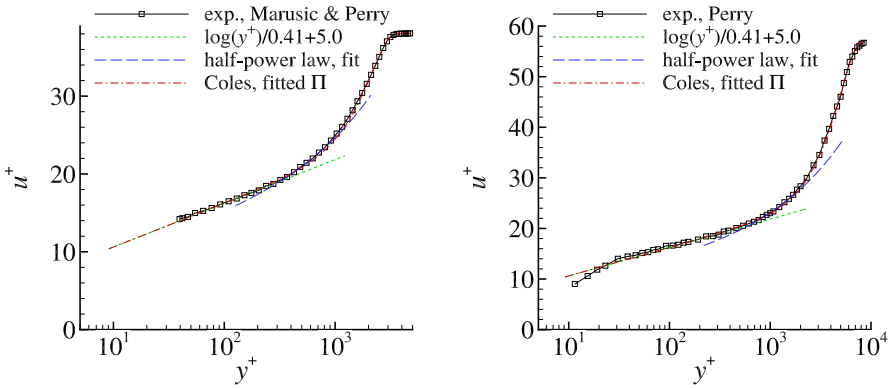

Figure 5.1: Left: Marusic & Perry at $\Delta p_s^+ = 7.17 \times 10^{-3}$ and $Re_\tau = 3406$. Right: Perry (ID 2907) at $\Delta p_s^+ = 7.89 \times 10^{-3}$ and $Re_\tau = 7926$.

large values of Δp_s^+ are studied. For the equilibrium flow by Skare & Krogstad, the mean velocity profile at $\Delta p_s^+ = 0.012$, $Re_\theta = 49107$ and $Re_\tau = 5117$ is given in figure 5.2 (left). Finally, the mean-velocity profile for the DLR/UniBw

experiment I for $U_\infty = 12$m/s at $\Delta p_s^+ = 0.049$, $Re_\theta = 20784$ and $Re_\tau = 2376$ is shown in figure 5.2 (right).

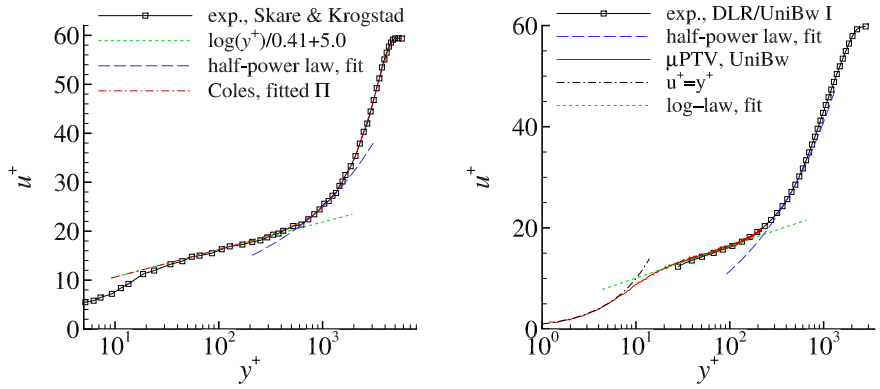

Figure 5.2: Left: Skare and Krogstad at station 4 at $\Delta p_s^+ = 0.012$ and $Re_\tau = 5117$. Right: DLR/UniBw flow I for $U_\infty = 12$m/s at $\Delta p_s^+ = 0.049$ and $Re_\tau = 2376$.

The log law in the mean velocity is found to be a robust feature for all flows. The region occupied by the log law is observed to be a large part of the inner layer for moderate values of Δp_s^+, but is found to be significantly smaller than 0.15δ for $\Delta p_s^+ > 0.01$. For y^+-values above the log-law region, the mean velocity turns upward above the log law and can be fitted by a half-power law. The upward turn above the log law in the inner layer is found to be increasing with increasing values of Δp_s^+. The increase of the upward turn can be described by the half-power law and its dependency on Δp_s^+. In the following, these qualitative observations are studied in more detail.

5.2 Reduction of the Log-Law Region

The question is as to whether the log-law region extends up to $y/\delta = 0.15$ as for ZPG. The results for $y_{\log,\max}/\delta$ versus Δp_s^+ are shown in figure 5.3 (left). Error bars for the individual test cases are included, as described in section 6.5. The log-law region extends up to $y/\delta = 0.15$ only for the equilibrium flows in a mild APG by Bradshaw and Clauser (see figure 5.3 (left)). For the equilibrium flows in a larger APG by Bradshaw, Clauser, and Skare & Krogstad, $y_{\log,\max}/\delta$ is found to be reduced already at the first measurement position in the APG region.
Next, consider the flows which evolve from a region of almost ZPG and then enter the APG region. These are the flow by Ludwieg and Tillmann in a mild APG, the flows B and E by Schubauer & Spangenberg, the flow by Marusic & Perry, and the flow by Schubauer & Klebanoff. For these flows, the outer edge of the log law is near 0.15δ in the ZPG region, and a clear reduction is already found at the first measurement station in the APG region (see figure 5.3 (left)). In the flow by Marusic & Perry, the first measurement station is in the ZPG region with $y_{\log,\max} = 0.14\delta$, whereas, at the next measurement station in the APG region, $y_{\log,\max}/\delta$ is found to be reduced to 0.1. For the flow by Schubauer

& Klebanoff, the flow is initially at an FPG over a streamwise length of 8 ft, then develops at almost ZPG over a length of 10 ft before entering into the APG region. In the rear part of the ZPG region, the thickness of the log-law region is larger than 0.15δ in the ZPG region, and $y_{\log,\max}/\delta$ is reduced to 0.1 at the first station in the APG region. For the flow by Ludwieg & Tillmann in a mild APG, a continuous reduction of $y_{\log,\max}/\delta$ in streamwise direction is found from initially 0.15 to values below 0.08. For the flow by Perry, $y_{\log,\max}/\delta$ is around 0.1 at the first measurement station which is already located in the APG region at $\beta_{\mathrm{RC}} = 2.3$.
The DLR/UniBw experiment necessitates some additional comments. The flow passes a region of mild convex curvature and streamwise changing pressure gradient from favourable to adverse before entering the APG focus region, Here the mean-velocity profile for u^+ shows a significant deviation from the log law even below $y^+ = 200$ and a remarkably large reduction of the log-law region (see figures 13 and 14 in Knopp et al. [2021]). Therefore, the low values found for $y_{\log,\max}/\delta$ are supposed to be influenced by history effects.

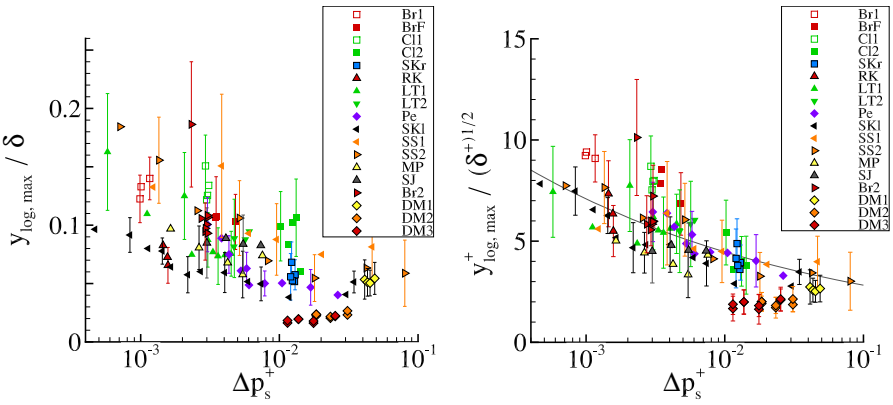

Figure 5.3: Reduction of the extent of the log-law region in an APG in two different scalings.

To summarise, the values for $y_{\log,\max}/\delta$ are found to be decreasing with increasing values of the pressure-gradient parameter, both in terms of Δp_s^+ and β_{RC}. The overall observation is that $y_{\log,\max}/\delta$ is below 0.11 for $\Delta p_s^+ > 0.005$ and $\beta_{\mathrm{RC}} > 4.5$, and below 0.08 for $\Delta p_s^+ > 0.015$ and $\beta_{\mathrm{RC}} > 12$.

Chapter 6

Correlations for a Wall Law

Now the aim is to describe the empirical correlations of the wall law. The functional form of the correlations is described in 6.1 The final calibration is based on a data fit. The correlations are described in sections 6.2 and 6.3. The analysis of the slope coefficient K of the half-power law (2.12) is given in section 6.4. The uncertainties are estimated and discussed in section 6.5.

6.1 Theoretical Considerations

The functional form of the correlations is prompted by two heuristic arguments, i.e., a similarity argument and a scaling argument.

6.1.1 Similarity Arguments

The first step is to find the basic functional dependency using arguments from the self-similarity analysis in section 2.5. From this analysis, it is expected that $y^+_{\log,\max}$ will depend on the Reynolds number and on the pressure-gradient parameter, in agreement with Yaglom [1979], Wei et al. [2005a], and Klewicki et al. [2009]. The first assumption is that β_H is the most important parameter for the solution of (2.21). Note that the precise definitions of the parameters in (2.22) are still open due to the question of a self-similar scaling for the Reynolds stresses. As a remedy, an empirical data analysis is pursued. Consider the reduced Hartree parameter

$$-\beta_{\mathrm{H,red}} = \Delta p_s^+ \, Re_\tau^2 \tag{6.1}$$

based on (2.23). This neglects the influence of u_τ/U_e. Note that u_τ/U_e is expected to be relevant for the outer layer as it determines the wake factor Π. For the inner layer, the influence of u_τ/U_e is assumed to be small at the moment. The functional dependency of the log law and the half-power law is irrespective of its formulation in terms of $u^+(y^+)$ and $f'(\eta)$. Strict self-similarity in the entire boundary layer would imply the existence of a correlation $\eta_{\log,\max}(\beta_{\mathrm{H,red}})$ as well as for $\eta_{\mathrm{sqrt,min}}$. Then the following ansatz is made

$$\eta_{\log,\max} = \frac{y^+_{\log,\max}}{Re_\tau} = C\beta^q_{\mathrm{H,red}} = CRe_\tau^{2q}\left(\Delta p_s^+\right)^q \tag{6.2}$$

with $q \in \mathbb{R}$ to be determined. The next idea is to determine the value of s (later being related to q) so that the plot of $y^+_{\log,\max}/Re^s_\tau$ versus Δp^+_s gives the least amount of spreading among the flows at different Re_τ in the database. This prompts the assumption $y^+_{\log,\max} \sim Re^s_\tau$. Then q can be inferred from

$$\eta^+_{\log,\max} = CRe^{2q}_\tau \left(\Delta p^+_s\right)^q = \frac{y^+_{\log,\max}}{Re_\tau} \sim Re^{s-1}_\tau \quad \Leftrightarrow \quad q = \frac{s-1}{2}\,. \tag{6.3}$$

The least amount of spreading was found for $s = 1/2$ (see figure 5.3 (right) and Knopp et al. [2022]), in agreement with the Re_τ-dependency found in Wei et al. [2005a], Klewicki et al. [2009], Romero et al. [2022]. The intermediate result is

$$y^+_{\log,\max} = CRe^{2q+1}_\tau \left(\Delta p^+_s\right)^q, \qquad q = -\frac{1}{4}\,. \tag{6.4}$$

6.1.2 Scaling Arguments

The simplification of using (6.1) neglects an additional Re-dependence involved in u_τ/U_e. Therefore, (6.4) is revisited and modified using the ansatz

$$y^+_{\log,\max} = CRe^{2q'+1}_\tau \left(\Delta p^+_s\right)^{q''} \tag{6.5}$$

with $s = 2q' + 1$. A relation for q'' can be found from a scaling argument. Consider the boundary-layer parameters in the modified scaling for the inner layer (see section 2.4) for the Reynolds number based on u_T

$$\delta^+_\mathrm{T} = \frac{\delta u_\mathrm{T}}{\nu} = \delta^+ \frac{u_\mathrm{T}}{u_\tau} \tag{6.6}$$

and for the pressure-gradient parameter in the modified inner scaling

$$\Delta p^+_{s,\mathrm{T}} = \frac{\nu}{\rho u^3_\mathrm{T}} \frac{\mathrm{d}P_w}{\mathrm{d}s} = \Delta p^+_s \left(\frac{u_\tau}{u_\mathrm{T}}\right)^3 = \left(\frac{u_p}{u_\mathrm{T}}\right)^3 . \tag{6.7}$$

When approaching separation, $\Delta p^+_{s,\mathrm{T}} \to 1/Re_c = 1/12$ due to (2.18) and does not approach infinity. Similarly $\delta^+_\mathrm{T} \to Re^{1/3}_c \delta u_p/\nu$ does not go to zero. Written in modified inner scaling, relation (6.5) becomes

$$y^+_{\log,\max,\mathrm{T}} = CRe^{2q'+1}_\mathrm{T} (\Delta p^+_{s,\mathrm{T}})^{q''} \left(\frac{u_\tau}{u_\mathrm{T}}\right)^{2q'-3q''} . \tag{6.8}$$

The explicit dependence on u_τ/u_T disappears if $q'' = 2q'/3$. The choice $q' = -1/4$ based on $s = 1/2$ leads to $q'' = -1/6$. Note that the dependency on $(u_\mathrm{T}/u_\tau)^{-2q'+3q''}$ is only mild for $q'' = -1/5$ (with $-2q' + 3q'' = -0.1$) and $q'' = -0.13$ (with $-2q' + 3q'' = 0.11$) found below.

6.2 The Extent of the Log-Law Region

Motivated by these heuristic arguments, we obtained the final calibration mainly from the data fit, which is shown in figure 5.3 (right)

$$y^+_{\log,\max} = 1.78 Re^{1/2}_\tau \left(\Delta p^+_s\right)^{-1/5}. \tag{6.9}$$

Note the change of the correlation (6.9) compared to the prior work in Knopp [2016], due to a revised analysis of the database and accounting for Re-effects. The variability of the data points and possible reasons for the deviation from (6.9) are discussed in sections 7.1, 7.2, and 7.3. The variability is due, on the one hand, to the uncertainty in the data and in the method used to determine the extent of the log-law region, and, on the other hand, to possible additional physical effects and parameters beyond Δp_s^+ and Re_τ unaccounted for in (6.9).

6.3 Variation of the Half-Power Law Region

The correlation for the beginning of the half-power law region is obtained in a similar manner to that employed for (6.9), using a data fit and guided by the heuristic arguments above. The same dependency on Re_τ as in (6.9) is used. The dependency on Δp_s^+ is a compromise due to the spreading in the data. The correlation becomes

$$y^+_{\mathrm{sqrt,min}} = 4.05 Re_\tau^{1/2} \, (\Delta p_s^+)^{-0.13} \, . \tag{6.10}$$

The result is shown in figure 6.1 (left). Large symbols are used to highlight the data sets used with the highest priority for the calibration. Additional data are needed for $\Delta p_s^+ < 0.002$ and $\Delta p_s^+ > 0.03$ at high Re.

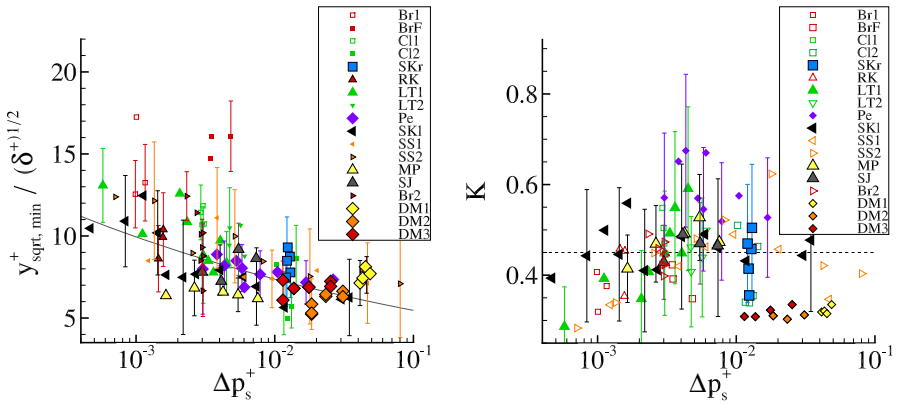

Figure 6.1: Variation of $y^+_{\mathrm{sqrt,min}}/(\delta^+)^{1/2}$ (left) and results for K (right) using large filled symbols to highlight the data sets used for the calibration.

6.4 The Slope Coefficient of the Half-Power Law

In the half-power law (2.12), the question is as to whether K can be described by a constant or follows a functional dependency, e.g., $K = f(\Delta p_s^+)$. For each profile of the database, the value for K was determined by a least-squares fit of (2.12) to the experimental data in the half-power law region. Note that K depends on the choice for α^+ in (2.12). As in all the present work, $\alpha^+ = \Delta p_s^+$ is used both for equilibrium flows and streamwise evolving flows. The results for K are shown in figure 6.1 (right). The data sets used for the calibration (SKr, SKl, MP, SJ, LT1) satisfy all criteria C1-C4 and are plotted using large

filled symbols. The data sets by Perry and the DLR/UniBw experiments are considered at a lower priority, due to supposed history effects, and are plotted using small filled symbols. The other data sets not used for the calibration are plotted using open symbols. The values for K are found to scatter around a value of $K = 0.45 \pm 0.15$. The variability in K is assumed to be due, on the one hand, to an uncertainty in the data and in the method of determining K (see section 6.5), and possibly, on the other hand, to differences in the flow characteristics (see sections 7.1-7.3).
For comparison, values reported in the literature for flows with non-zero skin friction are $K = 0.48 \pm 0.03$ in Townsend [1961], $K = 0.48$ in Perry [1966], and values between 0.41 and 0.51 in Szablewski [1960]. For large values of $\Delta p_s^+ \delta^+$, values reported are $K = 0.447$ in Kader and Yaglom [1978] and $K = 0.57$ in Afzal [2008]. Note that the values obtained for K depend on the form of the half-power law, i.e., (2.12) or (2.13), and on the region used for the least-squares fit. For example, if the half-power law fit is applied above the log-law region, as proposed by Perry [1966], then smaller values are obtained than if the fit is applied to all data in the inner layer above the buffer layer, as used e.g. by Afzal [2008]. Different proposals for a functional dependency of K by Kader and Yaglom [1978] and Afzal [2008] were tested, but did not lead to a smaller spreading in the results.
To summarise, a constant value for $K = 0.45 \pm 0.15$ is advocated, whose magnitude is congruent with previous findings in the literature.

6.5 Discussion of the Uncertainties

The variability of the results due to the uncertainty in the data and in the method for the data evaluation needs to be studied. First the uncertainties for $y^+_{\mathrm{log,max}}$ and $y^+_{\mathrm{sqrt,min}}$ are discussed. The first aspect is the uncertainty due to the distance Δy^+ between adjacent data points, which is given by the resolution of the measurement. The second aspect is the uncertainty due to the wiggles of the individual data points within each mean-velocity profile, i.e., their spreading around a smooth profile curve, leading to an additional contribution to the uncertainties.
The results for the extent of the log-law region with the estimated uncertainty bars are shown in figure 5.3 (right). For each mean-velocity profile, the deviation of the most likely value for $y^+_{\mathrm{log,max}}$ from the minimum and maximum possible value was determined, yielding the basic uncertainty. Additional contributions to the error bars are an estimated relative uncertainty of 10% in δ, of 6% in u_τ, and of 1% in ν. The correlation is within or close to the uncertainty bars for most of the profiles except for the flows Br1, BrF, Cl1, DM2, and DM3. The results for the beginning of the half-power law region with the estimated error bars are shown in figure 6.1 (left). The deviations will be discussed below in subsections 7.1, 7.2, and 7.3.
Concerning the variability of K, two contributions are studied. The first aspect is the uncertainty of Δp_s^+, which affects the value inferred for K. A relative uncertainty for Δp_s^+ of 25% was assumed, corresponding to an average relative uncertainty of 5% in $\mathrm{d}P/\mathrm{d}s$, of 6% in u_τ and of 1% in ρ and ν. A Monte-Carlo type approach yields an uncertainty of up to 11% for K. The second aspect is the lower and upper bound used for the half-power law fit. This was varied by

adding and/or removing the first and/or the last data point in the half-power law region using a Monte-Carlo type approach. This uncertainty was found to become large for profiles having a small number of data points in the half-power law region and for profiles exhibiting discernible oscillations. The details of the uncertainty estimates are described in appendix A.
The values for K with the error bars are shown in figure 6.1 (right). The spreading of the data points for K is within the uncertainty bars. The values for the flow by Perry are found to be larger than $K = 0.45$, whereas the values for the DLR/UniBw flows are smaller than for most of the other flows. This difference indicates that the value of K could be influenced by additional physical effects. This issue is discussed in sections 7.1 and 7.3.
To summarise: the spreading of the data around the correlations (6.9), (6.10) and around $K = 0.45$ occurs mostly within the uncertainty bars. The deviations for the DLR/UniBw flow II will be studied in detail in subsection 7.3.

Chapter 7

Discussion of the Wall Law

Some aspects and issues of the wall law are worth discussing. These are the subject of this section. The conjecture of a local wall law is described and discussed in section 7.1. Higher-order local effects and history effects are studied in section 7.2. The influence of the measurement accuracy improvement between the oldest and the more recent data and the comparison with data for low-Re flows are studied in section 7.3. The question of the breakdown of the log law law-of-the-wall is discussed in section 7.4. Finally, the log-law/half-power-law is compared to the law-of-the-wall/law-of-the-wake in section 7.5.

7.1 Conjecture of a Local Wall Law

The main conjecture is the existence of a wall law for the mean velocity in the inner layer, which is governed mainly by local parameters and whose leading order effects can be described by Δp_s^+ and Re_τ. Here Re_τ is considered as a local parameter, as it depends on the local value of δ, albeit δ is not a quantity of the near-wall flow and depends on the flow history. The need for Re_τ is described in the work by Wei et al. [2005a] and Klewicki et al. [2009]. Higher-order effects are assumed to slightly alter the wall law. Higher-order local effects are the mean flow acceleration described by the parameter $\Delta u_{\tau,s}^+$, and the effects of an increasing or decreasing APG, described by $\Delta^2 p_s^+$ based on $\mathrm{d}^2P/\mathrm{d}s^2$. The local flow parameters and their order of importance can be inferred from the models for the total shear stress (see section 2.2). The first-order approximation is the linear stress distribution $\tau^+ = 1 + \Delta p_s^+ y^+$, and Δp_s^+ appears as the leading order parameter. The deviation from the linear relation is due to the contribution of the mean-inertia term. The relative importance of the mean-inertia term increases with increasing y^+. Therefore $\Delta u_{\tau,s}^+$ is interpreted as a second-order parameter. Additional higher-order effects can be inferred from (**??**) and involve the parameter $\Delta^2 p_s^+$.
History and non-equilibrium effects can cause additional changes of the wall law. In streamwise evolving flows, the changing flow parameters can cause an imbalance between the different terms in the mean momentum equation. History effects are due to the finite response time of the flow to imbalancing effects (see Gungor et al. [2016]). The response time of the mean flow is different in the different regions of the boundary layer, and the mean-velocity profile is

the cumulative result of local conditions and history effects (see Gungor et al. [2016]). An attempt to describe the response time of the local mean flow uses the eddy turn-over time $T_{\mathrm{t.o.}} = \kappa y/u^*$ (see Sillero et al. [2013]). The eddy turn-over length $\delta_{\mathrm{t.o.}} = UT_{\mathrm{t.o.}}$ is the streamwise travelling distance of the local mean flow $U(y)$ within $T_{\mathrm{t.o.}}$. By using $u^* = \tau^{1/2}$ based on the total shear stress τ in conjunction with (2.8), the following estimate for $\delta_{\mathrm{t.o.}}$ as a multiple of δ at the wall-distance $\eta = y/\delta$ can be obtained

$$\frac{\delta^+_{\mathrm{t.o.}}(\eta)}{\delta^+} = \frac{\kappa u^+ \eta}{(1+\alpha^+\eta\delta^+)^{1/2}} \,. \tag{7.1}$$

Following Sillero et al. [2013], the flow tends to relax to equilibrium within $2\tau_{\mathrm{t.o.}}$. The evaluation of $\delta_{\mathrm{t.o.}}/\delta$ using (7.1) leads to the estimate $2\delta_{\mathrm{t.o.}} \approx \delta$ for $\eta = 0.1$ and $2\delta_{\mathrm{t.o.}} \approx 2\delta$ for $\eta = 0.2$ for $\Delta p_s^+ \gtrapprox 0.004$. This leads to the assumption that the flow in the inner layer relaxes rapidly, although not instantaneously. History effects are expected to be more relevant in the half-power law region than in the log-law region. The outer part of the inner layer can be influenced by history effects of the outer layer, given that the inner and outer layers are connected by an overlap region and that history effects are more prominent in the outer layer. In the outer layer, significant development distances are required for the large-scale turbulent motion to adjust to the local pressure-gradient conditions and for the mean flow to "forget" perturbations (see Marusic et al. [2015]), and the prior path of β_{RC}-values was found to be relevant for the history effects (see Bobke et al. [2017] and Vila et al. [2017], and Vila et al. [2020]).
The conjecture of a local wall law, the systematic reduction of the log-law region, and the appearance of a half-power law above the log law for turbulent boundary-layer flows are seen to be in concurrence with the findings for Couette-Poiseuille (CP) flow by Telbany and Reynolds [1980] and Nakabayashi et al. [2004], as described in the introduction. Note that CP flow is a self-similar flow in dynamic equilibrium within the meaning of Gungor et al. [2016]. This supports the proposition that the wall law is a first-order effect of the pressure gradient and not a history effect, given the applicability of the "moving-equilibrium" concept, as described in section 7.2.
Another issue is the onset of reverse flow as discussed in Alving et al. [1990]. In the experiment by Dengel and Fernholz [1990] the occurrence of the first reverse-flow events was found to coincide with the vanishing of the log law, whereas in the modified experiment Alving et al. [1990] the lack of a logarithmic region appeared to be caused by the strong Δp_s^+-value.

7.2 Discussion of Higher-Order Local and History Effects

The variability of $y_{\mathrm{log,max}}$, $y_{\mathrm{sqrt,min}}$ and K due to possible higher-order local effects depending on, e.g., $\Delta u^+_{\tau,s}$ and $\Delta^2 p_s^+$, and history effects is discussed. The question is whether any systematic trends can be found.
For this purpose, the data of figure 5.3 (right) are depicted again in figure 7.1 using two highlighted groups of data for greater clarity. The equilibrium flows are highlighted in figure 7.1 (left) and the streamwise evolving flows are highlighted in figure 7.1 (right). The highlighted data sets are plotted using large

symbols and include error bars, whereas the other data sets are plotted using small symbols and without error bars.

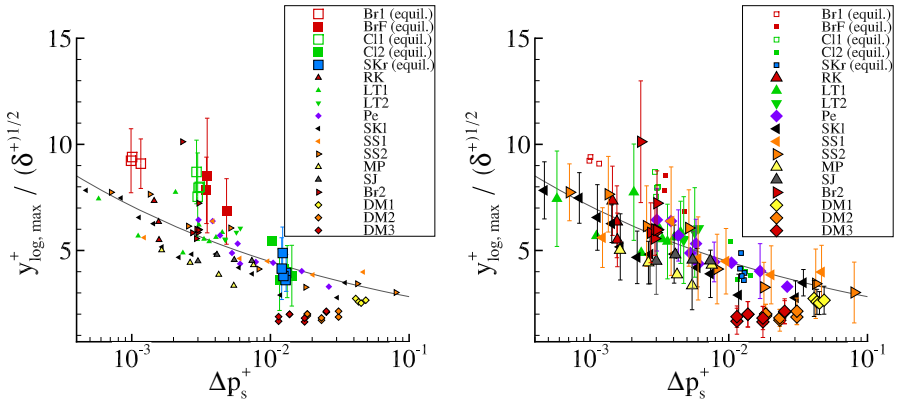

Figure 7.1: Reduction of the log-law region highlighting in large symbols the equilibrium flows (left) and the streamwise evolving flows (right) for the data of figure 5.3 (right).

The variability of the extent of the log law is studied first. The equilibrium flows in a mild APG show slightly larger values for $y^+_{\mathrm{log,max}}/(\delta^+)^{1/2}$ compared to the streamwise evolving flows in a mild APG (see figure 7.1 (left)). Streamwise evolving flows are at larger negative values of $\Delta u^+_{\tau,s}$ than equilibrium flows (see (2.24)), implying an increased relative importance of mean inertia. However, similar differences cannot be observed for $\Delta p_s^+ > 0.01$. Moreover, a clear effect of $\Delta^2 p_s^+$ cannot be identified from the flows by Perry and by Samuel & Joubert. For the variability of $y^+_{\mathrm{sqrt,min}}/(\delta^+)^{1/2}$, similar observations can be made.
The significantly lower values found for $y^+_{\mathrm{log,max}}/(\delta^+)^{1/2}$ for the two DLR/UniBw experiments are supposed to be due to history effects originating from a region of convex curvature and streamwise changing pressure gradient upstream of the APG region. Note that the ratio of δ to the radius of curvature was increased by a factor of two in the DLR/UniBw experiment II compared to the experiment I. This could explain the larger effects observed for the experiment II. The role of the measurement accuracy is discussed in section 7.3.
The variability of K in figure 6.1 (right) is supposed to be attributed to both higher-order local and history effects. Both are expected to be increasing with increasing wall-distance. Equilibrium flows and streamwise evolving turbulent boundary-layer flows cannot be clearly distinguished. The largest values for K are found for the flow by Perry Perry [1966]. The values at the first three stations (which are at the lowest Δp_s^+-values) could be influenced by history effects due to the flow acceleration upstream of the APG region. The measurements are on a 5 m-long flat plate at an incidence angle of 9.5° in the centre of the wind tunnel. The flow is expected to be strongly accelerated in the leading-edge region, before entering the APG region. This could lead to history effects. Further downstream, the relatively large values for K could be influenced by the upstream values of K, as well as by the decreasing APG, indicating a possible effect of $\mathrm{d}^2P/\mathrm{d}s^2$. For the DLR/UniBw experiment, the relatively small values for K are supposedly due to history effects of the upstream region of streamwise convex curvature and streamwise changing pressure gradient as well as the re-

laxation from curvature in conjunction with the streamwise changing pressure gradient from favourable to adverse. Moreover, the outer part of the inner layer and hence parts of the half-power law region are probably influenced by history effects of the outer layer.
To summarise, no systematic trends of the variability of $y_{\log,\max}$, $y_{\mathrm{sqrt},\min}$ and K on higher-order local effects can be found. History is found to have an effect, but more data sets are needed to find systematic trends. This leads to the conclusion that a more refined model than (6.9), (6.10) cannot be found given the uncertainties of the present data sets.
Finally, it is worth to comment on flow situations, for which substantial deviations from the local wall law can be expected. A rapid change in u_τ or in the pressure gradient over a short streamwise distance compared to δ (see Spalart [2010]) is expected to cause a significant departure from the "moving-equilibrium" state. Another situation beyond the scope of the present wall law is the initiation and growth of a new internal boundary layer beneath an existing turbulent boundary layer due to an abrupt change of surface curvature (see Baskaran et al. [1987]).

7.3 Measurement Accuracy and Low-Re Effects

The values for $y^+_{\log,\max}/(\delta^+)^{1/2}$ for the DLR/UniBw data are found to be significantly lower than for the other flows. Although a physical explanation for this can be given, it is worthwhile to investigate as to whether, between the oldest and the more recent data, there is also an influence of the measurement accuracy improvement. For this purpose, the results of figures 6.1 and 7.1 are revisited. The more recent experimental data sets by Skare & Krogstad, Marusic & Perry, Samuel & Joubert and the DLR/UniBw flows are highlighted in figure 7.2 (left) using large symbols. Moreover, the DNS data by Coleman et al. Coleman et al. [2018] and the experiment by Nagano et al. Nagano et al. [1991] at low Re are included and highlighted. The dashed line is for the value $C = 1.78$ found in (6.9). The dash-dotted line is for $C = 1.68$, which is only a small modification to improve the agreement with the highlighted data. The first conclusion is that the correlation is useful over a large range of Re, as the low-Re data are close to the high-Re data. The second conclusion is the suggestion that the constant in (6.9) be changed to $C = 1.68$.
Now the role of the measurement accuracy and the details of the method to determine $y^+_{\log,\max}$ are studied. On the one hand, the number of data points in the log-law region is increased for the more recent data. For example, Marusic & Perry achieved 13 data points in the log-law region below $y^+_{\log,\max} = 252$ at $\Delta p_s^+ = 7.5 \times 10^{-3}$ compared to four points for Schubauer & Spangenberg (flow E) at a similar Δp_s^+. This difference is due to the improvements of the measurement probes, and to considering lower values for Re. The larger number of data points gives a more critical view on the r.m.s. deviation between the u^+-profile and the log law. This can lead to smaller values for $y^+_{\log,\max}$.
To illustrate, consider the DLR/UniBw flow II data for $U_\infty = 36\,\mathrm{m/s}$. The results denoted by DM3v use an enlarged interval for the least-squares fit of u^+ to the log law up to $y^+ = 250$ (see table B.1). The idea is to emulate possible effects of the least-squares fit method used by Coles & Hirst. The increased interval yields larger values for $y^+_{\log,\max}/(\delta^+)^{1/2}$, reducing the deviation to the

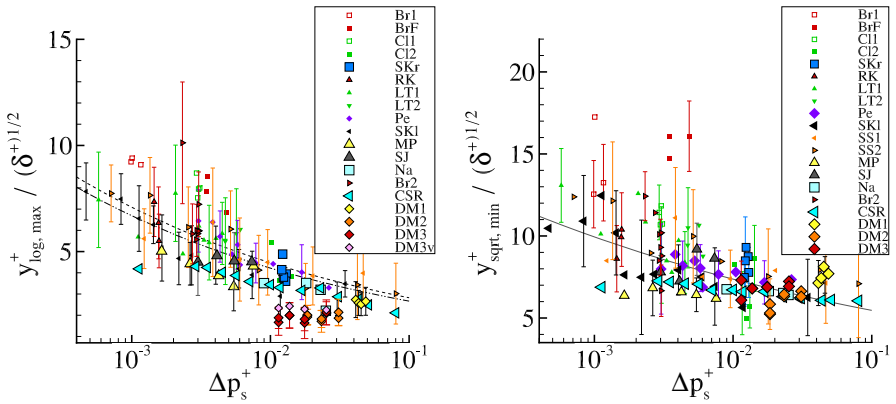

Figure 7.2: Influence of measurement accuracy on $y^+_{\mathrm{log,max}}/(\delta^+)^{1/2}$ (left, some acronyms omitted in legend) and of small Re for $y^+_{\mathrm{log,max}}/(\delta^+)^{1/2}$ (left) and $y^+_{\mathrm{sqrt,min}}/(\delta^+)^{1/2}$ (right).

other flows. However, this is at the cost of a larger r.m.s. deviation and hence questionable. It is concluded that the measurement accuracy can explain in parts the deviation of the DLR/UniBw data. However, such cannot explain the full deviation, indicating that additional physical effects are causing the large bulk of the deviation.

It is worth commenting on the use of $\kappa = 0.41$ and $B = 5.0$ for the older flows. An indirect method for u_τ might mask the subtle changes of κ and B in situations in which the mean velocity deviates from the universal log law (see Wei et al. [2005b]). Note that for the flows by Marusic & Perry and Samuel & Joubert, the agreement with the log law with $\kappa = 0.41$ and $B = 5.0$ is very good. However, this does not contradict the possible change of κ with Δp_s^+ proposed by Nickels [2004], as the relative change of κ would be only 4% for $\Delta p_s^+ < 0.0075$ according to Nickels [2004]. For the flows by Skare & Krogstad and by Perry, as well as that by Perry it cannot be decided whether fitted values for κ and B should be preferred over the values by Coles due to the wiggles in the u^+-profile. The changes of $y^+_{\mathrm{log,max}}$ if fitted values for κ and B are used, are well within the error bars. Moreover, for the old data, changes of κ and B could be masked by near-wall measurement errors in the mean velocity using Pitot tubes, as recently revealed by Bailey et al. [2013].

The results for $y^+_{\mathrm{sqrt,min}}/(\delta^+)^{1/2}$ for the low-Re flows are included in figure 7.2 (right). The data by Nagano and by Coleman et al. are highlighted using large symbols. They evince good agreement with the other data at moderate and high Re as well as with the correlation (6.10).

To summarise, the focus on the more recent data sets and the use of two flows at low Re confirm the results found in section 6. As a minor change, the constant C in (6.9) is changed from 1.78 to 1.68.

7.4 On the Breakdown of the Log Law for $\Delta p_s^+ > 0.05$

The hypothesis of the breakdown of the log law, if Δp_s^+ exceeds some threshold, e.g., $\Delta p_s^+ > 0.05$ (see Alving and Fernholz [1995]) is considered. The breakdown of the log law is understood here as the breakdown of a log-linear region $u^+ \sim \log(y^+)$, and is distinguished from a change of κ and B. Correlation (6.9) yields $y^+_{\log,\max} = 3.24(\delta^+)^{1/2}$ for $\Delta p_s^+ = 0.05$. This implies that the log law extends up to $y^+ = 92$ for $Re_\tau = 800$, indicating a rather thin region, whereas it extends up to around $y^+ = 162$ for $Re_\tau = 2500$ reached in the DLR/UniBw experiment I. Here, it is noteworthy that the outer edge of the log law in an APG from (6.9) is even smaller than the widely believed start of the log-law region in ZPG flows (see Wei et al. [2005a] andMarusic et al. [2013]).
Finally, note that the Thompson profile family Thompson [1967], a popular wall law of the 1960s, assumes the existence of the universal log law up to a fixed value of $y/\delta = 0.05$. The elevation of the Thompson profile above the log law is small below the y^+-values found from (6.9) (cf. figures 3 and 4 in Galbraith et al. [1977]).
To conclude, (6.9) is seen to be in agreement with the previous work by Alving and Fernholz [1995], Thompson [1967], and Galbraith et al. [1977].

7.5 Comparison with the Law-of-the-Wall/Law-of-the-Wake

Finally, it is worth discussing the log-law/half-power-law in comparison with the composite profile by Coles (4.1) (see Coles and Hirst [1969], Perry et al. [1994]). The latter is attractive, as it describes the mean-velocity profile across the entire boundary layer. Moreover, it can be used to derive a relation for the total shear stress (see Perry et al. [1994]) similar to (2.6), but ranging from the wall up to the boundary-layer edge. For the Coles wake parameter Π, different empirical correlations have been proposed to describe the effect of the pressure gradient. One example is the relation for Π being a function of β_{RC} and u_τ/U_e by Perry et al. [1994].
Regarding their descriptive accuracy, both the composite profile by Coles and the log-law/half-power-law can be fitted to the data in order to give a close agreement for equilibrium flows and for flows near equilibrium with moderate values of the pressure-gradient parameter. The log-law/half-power-law describes the experimental data up to 0.2δ and is found to be close to the composite profile by Coles for most mean-velocity profiles of the database. On the other hand, the blending of the log law and the half-power law is found to be more flexible for flows in a strong pressure gradient, significant effects of the mean-inertia term, and/or departure from equilibrium and history effects.
Another advantage of the half-power law compared to the wake function is that the latter requires an empirical correlation for Π to account for the upward turn of the mean-velocity profile above the log law. The upward turn is increasing with increasing magnitude of β_{RC} and Δp_s^+, and can be accounted for by making Π a function of, e.g., β_{RC} (see Perry et al. [1994]). On the other hand, the slope of the half-power law is already parametrised by Δp_s^+ and does not involve such

a calibration, as K can be described by a constant value for flows in "moving equilibrium" (see section 6.4).
The half-power law is attractive, as it provides a simple analytical relation for the mean-velocity gradient $\mathrm{d}U/\mathrm{d}y$ in wall-normal direction, which is the dominant contribution to a boundary-layer approximation and appears in the production term of the turbulent kinetic energy and in the equation for the turbulent dissipation ϵ and the specific rate of dissipation ω in statistical turbulence modelling based on the RANS equations.
Another advantage of the log-law/half-power-law is that it retains the log law unaltered. On the other hand, the wake contribution can be found to alter the mean velocity in the log-law region for strong values of the pressure gradient and large values of Π. However, any final assessment and conclusion are difficult, given the uncertainties in the data. To conclude, both approaches are seen to be complementary and have their own areas of application.

Chapter 8

Conclusion

An empirical wall law for the mean streamwise velocity for turbulent boundary-layer flows in an adverse pressure gradient is presented from a database analysis and from scaling and similarity arguments. The wall law describes the inner 20% of the boundary layer and is composed of a log law and a half-power law above the log law. For the slope coefficient of the half-power law K, a value of $K = 0.45 \pm 0.15$ is found, in agreement with previous findings in the literature. An empirical correlation for the reduction of the log-law region in ratio to the boundary-layer thickness is proposed. The leading order parameters are the pressure-gradient parameter Δp_s^+ and Re_τ. The results support the conjecture of the existence of a local wall law for the mean velocity and the moving equilibrium concept by Kader and Yaglom [1978]. Systematic changes of the wall law due to higher-order local effects and significant differences between equilibrium flows and streamwise evolving flows cannot be identified, given the uncertainties in the data. History effects are expected to be larger in the half-power law region than in the log-law region and contribute to the variability observed for K.

The correlation proposed for the erosion of the log-law region in an adverse pressure gradient can describe the hypothesis of the breakdown of the log law, if Δp_s^+ exceeds some threshold, e.g., $\Delta p_s^+ > 0.05$, as described by Alving and Fernholz [1995]. Moreover, the correlation implies that strict self-similarity of the mean-velocity profile in the inner layer cannot be expected, given the same value of the Rotta-Clauser pressure-gradient parameter β_{RC} alone, in agreement with the findings reported in Bobke et al. [2017], Vila et al. [2017], and Vila et al. [2020].

The correlation to describe the reduction of the log-law region in an adverse pressure gradient could also be of interest for experimental methods. The correlation could be used as an initial guess to identify the region of data points to which the Clauser-chart method can be applied to determine the friction velocity.

For future research, additional experimental data over a range of Reynolds numbers and pressure gradients would be greatly appreciated to support and to possibly improve the correlations found in the present work, in particular for mild pressure gradients and towards separation. Moreover, the wall law could be extended by accounting for non-equilibrium effects.

Acknowledgement

The DLR/UniBw experiment II was funded within the DFG-project "Analyse turbulenter Grenzschichten mit Druckgradient bei großen Reynoldszahlen mit hochauflösenden Vielkameramessverfahren" (Grant KA 1808/14-1 & SCHR 1165/3-1) and by the DLR Institute of Aerodynamics and Flow Technology. This work was funded by the DLR program directory board within the DLR internal projects VicToria and ADaMant. The author is very grateful to Per-Åge Krogstad, and to Sylvia Romero and Joe Klewicki for kindly providing their data, and to all the authors who have made their data available electronically or in documents. Additionally, the author would like to express his gratitude to Bernhard Eisfeld, Andreas Krumbein, Chris Willert, Andreas Schröder, Christian Kähler, Cord Rossow, and Philippe Spalart for numerous valuable discussions. The author would like to extend special thanks to Dieter Schwamborn, Cornelia Grabe, Michael Klein, Helmut Eckelmann, and Gert Lube. Finally, the valuable comments and suggestions by the reviewers are gratefully acknowledged.

Appendix A

Uncertainty Estimation

The uncertainty estimation for the slope coefficient K of the half-power law (2.12) is summarised in table A.1. The sensitivity of K on Δp_s^+ is found to be increasing from around 9 % for $\Delta p_s^+ = 0.005$ to 11 % for $\Delta p_s^+ = 0.015$. The sensitivity of K on the lower and upper bound of the interval I_{sqrt} used for the half-power law fit was studied using a Monte-Carlo type approach, where $\epsilon(I_{\text{sqrt}}) = \Delta y_i^+$ denotes the variation of I_{sqrt} by adding and/or removing one measurement point at the lower and/or upper bound of I_{sqrt}, as described in section 6.5. The values found for the confidence intervals for the levels 60%, 80%, and 95% are given in the table. The total uncertainty (denoted by ϵ_{sum}) is the sum of $\epsilon(\Delta p_s^+)$ and $\epsilon_{80}(I_{\text{sqrt}})$. As an exception, $\epsilon_{95}(I_{\text{sqrt}})$ is used for the flow by Marusic & Perry, due to the low values for this test case.

Table A.1: Uncertainty estimation for the method to determine K of the half-power law (2.12).

Author	ID	$\epsilon(K)$ due to $\epsilon(\Delta p_s^+)$=0.25	$\epsilon(K)$ due to $\epsilon(I_{\text{sqrt}}) = \Delta y_i^+$			Sum $\epsilon(K)$
			ϵ_{60}	ϵ_{80}	ϵ_{95}	ϵ_{sum}
Ludwieg & Tillmann, mild	1100	8.8 %	13.1 %	21.8 %	29.1 %	30.6 %
Ludwieg & Tillmann, strong	1200	9.1 %	13.7 %	20.8 %	39.0 %	29.9 %
Schubauer & Klebanoff	2100	11.2 %	11.0 %	21.8 %	23.1 %	33.0 %
Perry	2900	11.1 %	6.7 %	13.9 %	28.2 %	25.0 %
Samuel & Joubert	-	9.4 %	3.6 %	9.7 %	14.0 %	19.1 %
Marusic & Perry	-	9.5 %	3.1 %	5.0 %	8.5 %	18.0 %
Skare & Krogstad	-	10.9 %	5.8 %	16.9 %	28.9 %	27.8 %

Appendix B

Sensitivity Study of the Method for $y^+_{\log,\max}$

The sensitivity study described in section 4.2 for $y^+_{\log,\max}$ for the DLR/UniBw experiment at $U_\infty = 36\,\mathrm{m/s}$ is summarised in table B.1. The different values for $y^+_{\log,\max}$ were obtained by a variation of the interval $(y^+_{\min}, y^+_{\max})$ used to compute the least-square fit of the u^+-profile to the log law as described in section 4.2. The results for $y^+_{\log,\max}$ are given in the last column. The values obtained for κ and B from the fit are also given in the table.

Table B.1: Sensitivity study for $y^+_{\log,\max}$ for the DLR/UniBw experiment at $U_\infty = 36\,\mathrm{m/s}$.

U_∞ in m/s	x in m	Meas. techn. for U	Method for u_τ	Log law fit $y^+_{\min}$	Log law fit $y^+_{\max}$	κ (fit)	B (fit)	$y^+_{\log,\max}$ log law region
36	9.944	3D LPT	dir.	86	154	0.379	3.45	174
36	9.944	3D LPT	dir.	86	185	0.372	3.20	193
36	9.944	3D LPT	dir.	86	215	0.364	2.92	195
36	9.944	3D LPT	dir.	86	250	0.353	2.49	225
36	9.944	3D LPT	CCM	86	154	0.369	3.69	160
36	9.944	3D LPT	CCM	86	185	0.360	3.34	184
36	9.944	2D PIV	CCM	86	185	0.325	1.86	183
36	10.02	2D PIV	CCM	80	150	0.316	1.49	203
36	10.02	2D PIV	CCM	80	185	0.317	1.51	204
36	10.02	2D PIV	CCM	80	215	0.315	1.34	210
36	10.02	2D PIV	CCM	80	250	0.312	1.06	248

For $y^+_{\max} = 185$ the r.m.s. deviation is relatively small and u^+ follows the log law up to significantly larger y^+-values ($y^+_{\log,\max}$ up to 200) than used for the fit. For $y^+_{\max}$ up to 215, the changes of $y^+_{\log,\max}$ are much smaller than the changes of $y^+_{\max}$. For high values $y^+_{\max} = 250$, the r.m.s. deviation becomes larger and the increased values for $y^+_{\log,\max}$ are more questionable. The assessment of the r.m.s.

deviation is possible only thanks to the large number of data points in the log-law region and the smoothness of the data. Note that such is not possible for most of the old data sets in the database. The changes of $y^+_{\mathrm{log,max}}$ are much smaller than the changes in κ and B. The values for κ and B are adversely affected by the lower resolution of the 2D PIV method (compared to the highly-resolved 3D LPT data), by a too large interval for I_{fit}, and by the indirect method to determine u_τ (see Knopp et al. [2021]). Note that the resolution of the 2D PIV method was too low in the log-law region for an accurate determination of κ and B. If u_τ is determined from the CCM, then the $y^+_{\mathrm{log,max}}$-values are reduced by around 6%, due to the reduction of u_τ for the CCM compared to the direct method (see the results for $x = 9.944\,\mathrm{m}$ in table B.1).

Bibliography

N. Afzal. Turbulent boundary layer with negligible wall stress. *J Fluid Eng. – T. ASME*, 130:051205–1–15, 2008.

A. E. Alving and H. H. Fernholz. Mean-velocity scaling in and around a mild, turbulent separation bubble. *Phys. Fluids*, 7:1956–1969, 1995.

A. E. Alving, A. J. Smits, and J. H. Watmuff. Turbulent boundary layer relaxation from convex curvature. *J. Fluid Mech.*, 211:529–556, 1990.

S. C. C. Bailey, M. Hultmark, J. P. Monty, P. H. Alfredsson, M. S. Chong, R. D. Duncan, J. H. M. Fransson, N. Hutchins, I. Marusic, B. J. McKeon, H. M. Nagib, R. Örlü, A. Segalini, A. J. Smits, and R. Vinuesa. Obtaining accurate mean velocity measurements in high Reynolds number turbulent boundary layers using pitot tubes. *J. Fluid Mech.*, 715:642–670, 2013.

V. Baskaran, A. J. Smits, and P. N. Joubert. A turbulent flow over a curved hill. Part 1. Growth of an internal boundary layer. *J. Fluid Mech.*, 182:47–83, 1987.

A. Bobke, R. Vinuesa, R. Örlü, and P. Schlatter. History effects and near equilibrium in adverse-pressure-gradient turbulent boundary layers. *J. Fluid Mech.*, 820:667–692, 2017.

P. Bradshaw. The Response of a Retarded Equilibrium Turbulent Boundary Layer to the Sudden Removal of Pressure Gradient. Technical report, NPL Aero. Rep. 1145, 1965.

P. Bradshaw. The Turbulence Structure of Equilibrium Boundary Layers. Technical report, NPL Aero. Rep. 1184, 1966.

P. Bradshaw. The Response of a Constant-Pressure Turbulent Boundary Layer to the Sudden Application of an Adverse Pressure Gradient. Technical report, NPL Aero. Rep. 1219, 1967.

F. H. Clauser. Turbulent boundary layers in adverse pressure gradients. *J. Aeronaut. Sci.*, 21:91–108, 1954.

G. N. Coleman, S. Pirozzoli, M. Quadrio, and P. R. Spalart. Direct numerical simulation and theory of a wall-bounded flow with zero skin friction. *Flow, Turbul. Combust.*, 99:553–564, 2017.

G. N. Coleman, C. L. Rumsey, and P. R. Spalart. Numerical study of turbulent separation bubbles with varying pressure gradient and Reynolds number. *J. Fluid Mech.*, 847:28–70, 2018.

G. N. Coleman, C. L. Rumsey, and P. R. Spalart. Numerical study of a turbulent separation bubble with sweep. *J. Fluid Mech.*, 880:684–706, 2019.

D. Coles. The law of the wake in the turbulent boundary layer. *J. Fluid Mech.*, 1:191–226, 1956.

D. E. Coles and E. A. Hirst. *Computation of Turbulent Boundary Layers - 1968 AFOSR-IFP-Stanford Conference*. Thermosciences Division, Department of Mechanical Engineering, Stanford University, Stanford, California, USA, 1969.

P. Dengel and H. H. Fernholz. An experimental investigation of an incompressible turbulent boundary layer in the vicinity of separation. *J. Fluid Mech.*, 212:615–636, 1990.

W. J. Devenport and K. T. Lowe. Equilibrium and non-equilibrium turbulent boundary layers. *Prog. Aerosp. Sci.*, 131:100807, 2022.

S. A. Dixit and O. N. Ramesh. Pressure-gradient-dependent logarithmic laws in sink flow turbulent boundary layers. *J. Fluid Mech.*, 615:445–475, 2008.

K. Elsberry, J. Loeffler, M. D. Zhou, and I. Wygnanski. An experimental study of a boundary layer that is maintained on the verge of separation. *J. Fluid Mech.*, 423:227–261, 2000.

R. A. Galbraith, S. Sjolander, and M. R. Head. Mixing length in the wall region of turbulent boundary layers. *Aeronaut. Quart.*, 28:97–110, 1977.

A. G. Gungor, Y. Maciel, M. P. Simens, and J. Soria. Scaling and statistics of large-defect adverse pressure gradient turbulent boundary layer. *Int. J. Heat Fluid Flow*, 59:109–124, 2016.

J. O. Hinze. *Turbulence*. McGraw-Hill, USA, 1975.

R. Johnstone, G. N. Coleman, and P. R. Spalart. The resilience of the logarithmic law to pressure gradients: evidence from direct numerical simulation. *J. Fluid Mech.*, 643:163–175, 2010.

B. A. Kader and A. M. Yaglom. Similarity treatment of moving-equilibrium turbulent boundary layers in adverse pressure gradients. *J. Fluid Mech.*, 89: 305–342, 1978.

N. Kim and D. L. Rhode. Streamwise curvature effect of the incompressible turbulent mean velocity over curved surfaces. *J Fluid Eng. – T. ASME*, 122: 547–551, 2000.

V. Kitsios, A. Sekimoto, C. Atkinson, J. A. Sillero, G. Borell, A. G. Gungor, J. Jimenez, and J. Soria. Direct numerical simulation of a self-similar adverse pressure gradient turbulent boundary layer at the verge of separation. *J. Fluid Mech.*, 829:392–419, 2017.

J. C. Klewicki, P. Fife, and T. Wei. On the logarithmic mean profile. *J. Fluid Mech.*, 638:73–93, 2009.

T. Knopp. A new wall-law for adverse pressure gradient flows and modification of k-ω type RANS turbulence models. 2016. AIAA Paper 2016-0588.

T. Knopp. Experimental study of the inner layer of an adverse-pressure gradient turbulent boundary layer. Technical report, DLR IB 2019-74 (https://elib.dlr.de/130693/), 2019.

T. Knopp, N. A. Buchmann, D. Schanz, B. Eisfeld, C. Cierpka, R. Hain, A. Schröder, and C. J. Kähler. Investigation of scaling laws in a turbulent boundary layer flow with adverse pressure gradient using PIV. *J. Turbul.*, 16: 250–272, 2015.

T. Knopp, N. Reuther, M. Novara, D. Schanz, E. Schülein, A. Schröder, and C. J. Kähler. Experimental analysis of the log law at adverse pressure gradient. *J. Fluid Mech.*, 918:A17–1–32, 2021.

T. Knopp, M. Novara, D. Schanz, N. Reuther, W. Lühder, C. Willert, A. Schröder, E. Schülein, R. Hain, and C. J. Kähler. Modification of the SSG/LRR-ω RSM for adverse pressure gradients using turbulent boundary layer experiments at high Re. In *13th International ERCOFTAC Symposium on Engineering Turbulence Modelling and Measurements ETMM13, 15th - 17th September 2021, Rhodes, Greece*, Rhodes, 2022.

H. Ludwieg and W. Tillmann. Untersuchungen über die Wandschubspannung in turbulenten Reibungsschichten. *Ing.-Arch.*, 17:288–299, 1949.

Y. Maciel, T. Wei, and A. G. Gungor M. P. Simens. Outer scales and parameters of adverse-pressure-gradient turbulent boundary layers. *J. Fluid Mech.*, 844: 5–35, 2018.

I. Marusic and A. E. Perry. A wall-wake model for the turbulence structure of boundary layers. Part 2. Further experimental support. *J. Fluid Mech.*, 298: 389–407, 1995.

I. Marusic, J. P. Monty, M. Hultmark, and A. J. Smits. On the logarithmic region in wall turbulence. *J. Fluid Mech.*, 716:R3–1–R3–11, 2013.

I. Marusic, K. A. Chauhan, V. Kulandaivelu, and N. Hutchins. Evolution of zero-pressure-gradient boundary layers from different tripping conditions. *J. Fluid Mech.*, 783:379–411, 2015.

H. McDonald. The effect of pressure gradient on the law of the wall in turbulent flow. *J. Fluid Mech.*, 35:311–336, 1969.

G. L. Mellor. The effects of pressure gradients on turbulent flow near a smooth wall. *J. Fluid Mech.*, 24:255–274, 1966.

Y. Nagano, M. Tagawa, and T. Tsuji. Effects of adverse pressure gradients on mean flows and turbulence statistics in a boundary layer. In F. Durst, R. Friedrich, B. E. Launder, F. W. Schmidt, U. Schumann, and J. H. Whitelaw, editors, *Eighth symposium on turbulent shear flows, Technical University of Munich, September 9-11, 1991*, Berlin, 1991. Springer-Verlag.

K. Nakabayashi, O. Kitoh, and Y. Katoh. Similarity laws of velocity profiles and turbulence characteristics of Couette-Poisseuille turbulent flows. *J. Fluid Mech.*, 507:43–69, 2004.

T. B. Nickels. Inner scaling for wall-bounded flows subject to large pressure gradients. *J. Fluid Mech.*, 521:217–239, 2004.

V. C. Patel. Calibration of the Preston tube and limitations on its use in pressure gradients. *J. Fluid Mech.*, 23:185–208, 1965.

A. E. Perry. Turbulent Boundary Layers in Decreasing Adverse Presssure Gradients. *J. Fluid Mech.*, 25:481–506, 1966.

A. E. Perry, J. B. Bell, and P. N. Joubert. Velocity and temperature profiles in adverse pressure gradient turbulent boundary layers. *J. Fluid Mech.*, 25: 299–320, 1966.

A. E. Perry, I. Marusic, and J. D. Li. Wall turbulence closure based on classical similarity laws and the attached eddy hypothesis. *Phys. Fluids*, 6:1024–1035, 1994.

S. K. Romero, S. J. Zimmerman, J. Philip, C. White, and J. C. Klewicki. Properties of the inertial sublayer in adverse pressure-gradient turbulent boundary layers. *J. Fluid Mech.*, 937:A30–1–36, 2022.

J. Rotta. Über die Theorie turbulenter Grenzschichten. Technical report, Mitteilungen aus dem Max-Planck-Institut für Strömungsforschung Nr. 1. (Translated as: On the theory of turbulent boundary layers. NACA Technical Memorandum No. 1344, 1953.), 1950.

A. E. Samuel and P. N. Joubert. A boundary layer developing in an increasingly adverse pressure gradient. *J. Fluid Mech.*, 66:481–505, 1974.

G. Schubauer and P. Klebanoff. Investigation of Separation of the Turbulent Boundary Layer. Technical report, NASA TN 3244, 1950.

G. B. Schubauer and W. G. Sprangenberg. Forced mixing in boundary layers. *J. Fluid Mech.*, 8:10–32, 1960.

M. L. Shur, P. R. Spalart, M. Kh. Strelets, and A. Travin. A hybrid RANS-LES approach with delayed-DES and wall-modelled LES capabilities. *Int. J. Heat Fluid Flow*, 29:1638–1649, 2008.

J. A. Sillero, J. Jimenez, and R. D. Moser. One-point statistics for turbulent wall-bounded flows at Reynolds numbers up to $\delta^+ \approx 2000$. *Phys. Fluids*, 25: 105102–1, 2013.

P. E. Skare and P. A. Krogstad. A turbulent equilibrium boundary layer near separation. *J. Fluid Mech.*, 272:319–348, 1994.

P. R. Spalart. The Law of the Wall. Indications from DNS, and Opinion. In *Progress in Wall Turbulence: Understanding and Modelling. Proceedings of the WALLTURB International Workshop held in Lille, France, April 21-23, 2009*, pages 9–20, Dordrecht, 2010. Springer.

P. R. Spalart. Philosophies and fallacies in turbulence modeling. *Prog. Aerosp. Sci.*, 74:1–15, 2015.

B. S. Stratford. The prediction of separation of the turbulent boundary layer. *J. Fluid Mech.*, 5:1–16, 1959.

W. Szablewski. Turbulente Strömungen in divergenten Kanälen. *Ing.-Arch.*, 22: 268–281, 1954.

W. Szablewski. Analyse von Messungen turbulenter Grenzschichten mittels der Wandgesetze. *Ing.-Arch.*, 29:291–300, 1960.

M. M. M. El Telbany and A. J. Reynolds. Velocity distributions in plane turbulent channel flows. *J. Fluid Mech.*, 100:1–29, 1980.

F. Tessicini, N. Li, and M. Leschziner. Large-eddy simulation of three-dimensional flow around a hill-shaped obstruction with a zonal near-wall approximation. *Int. J. Heat Fluid Flow*, 28:894–908, 2007.

B. G. J. Thompson. A new two-parameter family of mean velocity profiles for incompressible turbulent boundary layers on smooth walls. Technical report, ARC R & M 3463, 1967.

A. A. Townsend. Equilibrium layers and wall turbulence. *J. Fluid Mech.*, 11: 97–120, 1961.

B. van den Berg. The law of the wall in two- and three-dimensional turbulent boundary layers. Technical Report NLR TR 72111 U, National Aerospace Laboratory NLR, Amsterdam, 1973.

B. van den Berg. A three-dimensional law of the wall for turbulent shear flows. *J. Fluid Mech.*, 70:149–160, 1975.

C. S. Vila, R. Örlü, R. Vinuesa, P. Schlatter, A. Ianiro, and S. Discetti. Adverse-pressure-gradient effects on turbulent boundary layers: Statistics and flow-field organization. *Flow, Turbul. Combust.*, 99:589–612, 2017.

S. Vila, R. Vinuesa, S. Discetti, A. Ianiro, P. Schlatter, and R. Örlü. Experimental realisation of near-equilibrium adverse-pressure-gradient turbulent boundary layers. *Exp. Therm. Fluid. Sci.*, 112:109975, 2020.

R. Vinuesa, A. Bobke, R. Örlü, and P. Schlatter. On determining characteristic length scales in pressure-gradient turbulent boundary layers. *Phys. Fluids*, 28:055101, 2016.

T. Wei, P. Fife, J. Klewicki, and P. McMurtry. Properties of the mean momentum balance in turbulent boundary layer, pipe and channel flows. *J. Fluid Mech.*, 522:303–327, 2005a.

T. Wei, R. Schmidt, and P. McMurtry. Comment on the Clauser chart method for determining the friction velocity. *Exp. Fluids*, 38:695–699, 2005b.

A. M. Yaglom. Similarity laws for constant-pressure and pressure-gradient turbulent wall flows. *Annu. Rev. Fluid Mech.*, 11:505, 1979.